Application of KAM Theorem to Earth Orbiting Satellites

THESIS

Bryan D. Little, Captain, USAF

AFIT/GA/ENY/09-M05

DEPARTMENT OF THE AIR FORCE
AIR UNIVERSITY

AIR FORCE INSTITUTE OF TECHNOLOGY

Wright-Patterson Air Force Base, Ohio

The views expressed in this thesis are those of the author and do not reflect the official policy or position of the United States Air Force, Department of Defense, or the United States Government.

AFIT/GA/ENY/09-M05

Application of KAM Theorem to Earth Orbiting Satellites

THESIS

Presented to the Faculty

Department of Aeronautical and Astronautical Engineering

Graduate School of Engineering and Management

Air Force Institute of Technology

Air University

Air Education and Training Command

In Partial Fulfillment of the Requirements for the

Degree of Master of Science in Astronautical Engineering

Bryan D. Little, BSA

Captain, USAF

March 2009

AFIT/GA/ENY/09-M05

Application of KAM Theorem to Earth Orbiting Satellites

Bryan D. Little, BSA
Captain, USAF

Approved:

William E. Wiesel, PhD (Chairman) — 13 Mar '09
Date

Lt Col Kerry D. Hicks, PhD (Member) — 13 Mar 09
Date

Nathan A. Titus, PhD (Member) — 13 Mar 09
Date

AFIT/GA/ENY/09-M05

Abstract

An orbit that lies on a Kolmogorov, Arnold, and Moser (KAM) Torus will remain on that torus until and unless it experiences a force that causes it to leave the torus. Earth satellites that are subject only to the Earth's gravity field may lie on such KAM tori. Analyzing on orbit satellite position data should allow for the identification of the fundamental frequencies needed to define the KAM tori for modeling Earth satellite orbits.

KAM Tori are created for the Gravity Recovery and Climate Experience (GRACE) and Jason-1 satellites to model their orbital motion. Precise position data for the satellites is analyzed using a modified Laskar frequency algorithm to determine the fundamental frequencies of the orbits. The fundamental frequencies along with a set of Fourier coefficients completely describe the tori. These tori are then compared to the precise orbital position data for the satellites to determine how well they model the orbits.

The KAM torus created for the Jason-1 satellite is able to represent the position of the satellites to within 1 km. Further refinement of the torus should be possible, resulting in a more accurate model of the orbit. The GRACE torus was less successful at determining the satellite positions. Atmospheric drag cannot be ignored at the altitude where GRACE flies. It may still be possible to model GRACE with a KAM torus by applying perturbation theory to the torus; however, further research is needed to confirm this.

Acknowledgements

First and foremost, I would like to thank my Lord and Savior, Jesus Christ, for all of his blessings. I would also like thank Dr Wiesel, for his guidance, instruction, and support as my research advisor and all of my committee members for their instruction during my numerous Astrodynamics classes. Thanks also to Maj Bordner for acting as a sounding board and a reality check. And finally, I must thank my wife, who has continued to be my biggest supporter and best friend throughout this work and my kids, for constantly reminding me that there was more than just school to keep me busy.

Bryan D. Little

Table of Contents

Page

Page

List of Figures

List of Symbols

List of Abbreviations

Application of KAM Theorem to Earth Orbiting Satellites

I. Introduction

Since the beginning of the space age, thousands of objects have been launched into orbit. However, unlike terrestrial and airborne systems that are moved to places where they are not going to interfere with ongoing operations, space systems continue to *float* in space until their orbit decays enough to reenter the atmosphere. Thus, there are still many non-operational systems flying in space, along with our operational systems. The US Space Surveillance Network (SSN) tracks these objects and attempts to accurately predict their future motion to ensure that high priority missions are not impacted.

1.1 Motivation

The standard method for orbit modeling starts with Kepler's solution to the Two Body Problem (2BP) and uses perturbation theory to account for some of the major error sources; these errors are due to effects like variations in the Earth's gravitational field. A common method begins with an initial condition, and the orbits are integrated forward in time. This is a computationally expensive process, which restricts the number of perturbations that can be included; for example, the Earth's oblateness effect is typically included, but other terms of the geopotential may be left out, especially when integrating large numbers of orbits. Other methods are analytical and use series expansions of the equations of motion, which include perturbations like the geopotential. These series expansions become very complex and must be truncated to make them easier to handle operationally. Orbital predictions created with these methods are only valid for a short time before they must be recalculated; the perturbations that are not accounted for, like the higher order gravitational variations, build up in the error over time.

1.2 Approach

A more accurate method for orbit determination could reduce the work required to track all of the objects orbiting Earth. This work attempts to show that the KAM theorem may be one such method that could be used to model satellite orbits.

The Kolmogrov-Arnold-Moser (KAM) theorem states that a nearly integrable Hamiltonian system subject to a small perturbation will lie on an invariant torus [9]; these tori have become known as KAM tori. Earth orbiting satellites may behave according to the KAM theorem since the 2BP is an integrable Hamiltonian system. Assuming the only perturbation source is the Earth's gravitational potential, which causes small, smooth perturbations to the 2BP [19], the criteria for KAM theorem is met.

The key to determining whether a system lies on a KAM torus lies in finding the fundamental frequencies of the torus [9]; the number of frequencies corresponds to the number of coordinates in the Hamiltonian. In the case of Earth orbiting satellites there are three fundamental frequencies: the anomalistic frequency (ω_1), the Earth rotation rate plus the nodal regression rate (ω_2) and the apsidal regression rate (ω_3). These frequencies can be identified from a Fourier transform of the orbital position data of a satellite. If the satellite's orbit lies on a KAM torus, the satellite position can be determined accurately for any point in the future, assuming no other external forces are encountered.

1.3 Problem Statement

This work looks at two satellite systems, the Gravity Recovery and Climate Experiment (GRACE) and Jason-1 satellites. Orbital data from each system is run through a modified Laskar Fourier transform algorithm to determine the fundamental frequencies of the orbit [10]. These frequencies and their corresponding Fourier series coefficients define the new coordinates for the Hamiltonian that describes the torus; the conjugate momenta can be found from the coordinates and their derivatives [20].

1.4 Results

Analysis shows that the Jason-1 satellite orbit can be modeled by a KAM torus to within 1 km of the real orbital data over a 30 day period. Further refinement may improve this accuracy. The torus for the GRACE satellite was not successful, due to the appearance of atmospheric drag in the data. It may still be possible to define the GRACE orbit with a KAM torus, if the torus can be modified to account for the atmospheric drag.

II. Background

This chapter begins with discussions of the GRACE and Jason-1 satellites. These satellites were chosen because the position data for each is accurately known. Accurate position data is needed to ensure the frequencies can be identified with as much accuracy as possible.

Current methods for orbit determination are also explained along with their drawbacks. The KAM theorem will be discussed in more detail, and past applications are presented. Finally, explanations of the orbital dynamics and the geopotential are given.

2.1 GRACE

The mission of GRACE is to measure the temporal and spatial variability of Earth's gravitational field. There are some advantages that make GRACE superior to previous methods for creating a gravity model: the use of identical satellites flying in formation along with accurate position measurements from onboard GPS receivers, accelerometer measurements, satellite attitude changes and inter-satellite range changes. All of these measurements allow GRACE to measure the finer effects of the gravity field that cannot be seen with an individual vehicle.

Both satellites were launched on 17 March 2002 into co-planar, near circular, polar orbits at 500 km altitude; the separation of the satellites is kept between 170 and 220 km, which requires a maneuver approximately every 30-60 days. Other than maintaining the separation of the satellites, the satellites are left to the natural effects of the gravity field and the orbits are allowed to decay; as of Aug 2007, the satellites semimajor axes had decayed approximately 27 km [1].

The GRACE-based Earth Gravity Model (EGM) is published approximately every 30 days. The accuracy of the model comes from the individual measurements of each satellite as well as the comparison of the measurements. The comparison of the satellite measurements is how the finer effects are determined; since the satellites pass over nearly the same position on Earth at slightly different times, the smallest

temporal and spatial variations of the gravity field will show up in the differences in the satellite measurements.

The measurements of the GRACE satellites have shown significant improvement in the EGM, for terms below about 110, over previous models such as EGM-96 [16]. The GRACE based EGM has also been combined with EGM-96 to create a full degree/order 360 model (EIGEN-CG01C) [16]. And yet, work continues to bring further improvement to the models.

2.2 Jason-1

The Jason-1 satellite carries on the mission of the Topex/Poseiden satellite. Radar altimetry is used to measure surface height of the world's ocean to an accuracy of 3.3 cm [3]; some of the other mission objectives include understanding ocean circulation and understanding how changes in the oceans and the atmosphere are related.

Jason-1 was launched on 7 December 2001 into a circular orbit at an inclination of 66° and a mean altitude of 1336 km. This allows for visibility of 90% of the world's oceans with a nominal repeat period of 10 days. Maneuvers are scheduled between repeat periods whenever possible to ensure the most continuity in measurements.

A key to obtaining accurate measurements of the ocean heights is knowing the orbital position of the satellite to high precision. For Jason-1, the orbital positions are obtained from a combination of Satellite Laser Ranging (SLR) and the Doppler Orbitography and Radio-positioning Integrated by Satellite (DORIS) tracking systems. This method is able to provide position data that is accurate to within 3 cm [3].

2.3 Modern Orbit Determination

The position data for the GRACE and Jason-1 satellites are quite precise, both being within a few centimeters. Unfortunately, these are only obtained after the satellite has passed through the given positions. Trying to predict a satellite's future

position to the same sort of accuracy is not currently possible for any extended length of time.

The methods that are used today to do orbit determination, prediction and modeling rely on numerical integration of the perturbed 2BP, or analytical solutions to the equations of motion. Numerical integration can be very computationally expensive and has a limit to the period of validity. In the past it could take as much time to numerically integrate an orbit as it took for the satellite to move through the orbit to the point to which you were integrating. As the speed of computers has increased, the time required to perform these integrations has decreased. However, at the same time, the number of orbits needing to be integrated has increased and the computational load remains high.

General analytical solutions of the equations of motion through series expansions are computationally less expensive than numerical integration of the orbit; the solution provides the osculating orbital elements as a function of time, which are used to determine future positions based on initial conditions [18]. Unfortunately, there is generally a high level of complexity in the series expansions. To reduce the complexity of the solution, the series are usually truncated after the first few terms. This also solves the problem of small divisors, which is common when dealing with orbits that have small eccentricities [17,18]; however, it introduces small error sources which build up in the solution over time.

Current orbit determination methods are also restricted by how far into the future they can model the orbit due to the buildup of errors in the accuracy. Because of the high computational load required for the integrations, the number of perturbations included is kept fairly low. For example the Earth's gravitational potential has been measured to degree and order 360, however, to reduce the computational load, the J2 term (which is the largest term in the geopotential) is almost always included, but depending on the computational load that can be handled, there may be no other terms included, or there may be quite a few other terms included. In the

analytical solution, this problem arises from the truncation of the series expansions. The magnitude of the terms beyond J2 are on the order of 10^{-6} and smaller, so this may not have a significant effect as long as the time period for the prediction is limited, but as the time increases the uncertainty of the solution increases and its validity decreases.

One area that is hindered by the current methods of orbit determination is the formation flying of satellites. Each satellite in a formation requires its own orbit model, which leads to its own level of uncertainty. Assuming the formation needs to stay within certain tolerances concerning separation and geometry, the problem becomes very difficult. A more accurate orbit determination method with a longer period of validity is needed to make formation flight of satellites more feasible.

2.4 Kolmogrov, Arnold, Moser Theorem

The KAM Theorem is the result developed by Kolmogrov [9], then proved by Arnold [2] and Moser [14], to describe the motion of a nearly integrable Hamiltonian system that is only subject to small, smooth perturbations. The Hamiltonian for such a system is given by

$$H_\varepsilon(I, \varphi) = h_o(I) + \varepsilon h(I, \varphi), \tag{2.1}$$

where h_o and h are real-analytic functions, ε is a small real parameter, and I and φ are symplectic action-angle variables. The theory states that such a system will lie on a torus that can be described by the fundamental frequencies of the orbit and associated Fourier series coefficients; an N-dimensional Hamiltonian will have N frequencies and will lie on a torus in 2N-dimensional phase space. This equality of the number of coordinates and frequencies is mandated by the Hamiltonian-Jacobi theorem.

KAM theorem has been shown to approximate well the Restricted, Circular, Planar, Three-Body Problem (RCPTBP), specifically the motion of asteroids under the effects of the Sun and Jupiter [5–7]. Celletti and Chierchia [6] showed that the

asteroid 12-Victoria, in a Keplerian orbit about the Sun and perturbed by Jupiter, could be modeled using the KAM theorem; in this case the perturbation is equal to the Jupiter-Sun mass ratio, $\varepsilon \approx 10^{-3}$. They were able to show that the results of their analysis agreed well with observed data for the system.

More recently, Wiesel [19] has shown that frequencies for Earth orbits could be identified, and the orbits could be fit to KAM Tori [13, 20]. Assuming the torus is exact, any trajectory that lies on the torus will remain on the torus in the future. This differs from perturbation theory, which is only an approximation of what will happen in the future and, therefore, must be updated due to error growth.

2.5 Orbital Dynamics

To apply the KAM theorem to Earth orbiting satellites, a reference frame must be chosen where the torus will be a static geometric structure; this means we need a coordinate frame that rotates with the Earth [19]. The Earth Centered Earth Fixed (ECEF) coordinate frame is chosen as the frame of reference for this work, and is defined with the x component through the Prime Meridian at the equator, the z component northward through the axis of rotation and the y component pointing in the right hand sense.

In the ECEF frame, the coordinates of the Hamiltonian are the positions x, y, and z and the momenta are equal to the inertial velocities resolved along the coordinate axes [19]. The momenta are given in Equation 2.2

$$\begin{aligned} p_x &= \dot{x} - \omega_{\oplus} y \\ p_y &= \dot{y} + \omega_{\oplus} x \\ p_z &= \dot{z} \end{aligned} \tag{2.2}$$

The Hamiltonian is found from $H = \sum_i p_i \dot{q}_i - T + V$; rearranging Equation (2.2), to get the time derivatives of the coordinates, and substituting back in gives

the Hamiltonian in terms of the coordinates and momenta only. The resulting Hamiltonian for Earth orbiting satellites is given by,

$$\begin{aligned} H = \frac{1}{2}(p_x^2 + p_y^2 + p_z^2) + \omega_\oplus(yp_x - xp_y) \\ - \frac{\mu}{r}\sum_{n=1}^{\infty}\sum_{m=1}^{\infty}\left(\frac{r}{R_\oplus}\right)^{-n} P_n^m(\sin\delta) \\ \times (C_{nm}\cos m\lambda + S_{nm}\sin m\lambda) \end{aligned} \tag{2.3}$$

where $R_\oplus$ is the equatorial radius of Earth, μ is the gravitational parameter, $\omega_\oplus$ is the rotation rate of the Earth and C_{nm} and S_{nm} are the gravity field coefficients. The P_n^m are the associated Legendre Polynomials, and r, δ and λ are the radius, geocentric latitude and east longitude of the of the satellite, respectively, and are defined in equation (2.4).

$$\begin{aligned} r &= \sqrt{x^2 + y^2 + z^2} \\ \sin\delta &= \frac{z}{\sqrt{x^2 + y^2}} \\ \tan\lambda &= \frac{y}{x} \end{aligned} \tag{2.4}$$

Notice, in this reference frame the Hamiltonian has no dependence on time and is thus a constant of the motion.

2.6 The Geopotential

For Earth orbiting satellites, the perturbation that is of interest in the application of the KAM theorem is the geopotential, which is due to the non-homogeneity of the planet. Figure 2.1 displays the differences between the theoretical geopotential of a smooth spherical Earth and the actual geopotential as measured by GRACE [1]. The areas where the potential is highest when compared to the smooth Earth are raised and colored red, while the areas of lowest potential are recessed and colored blue.

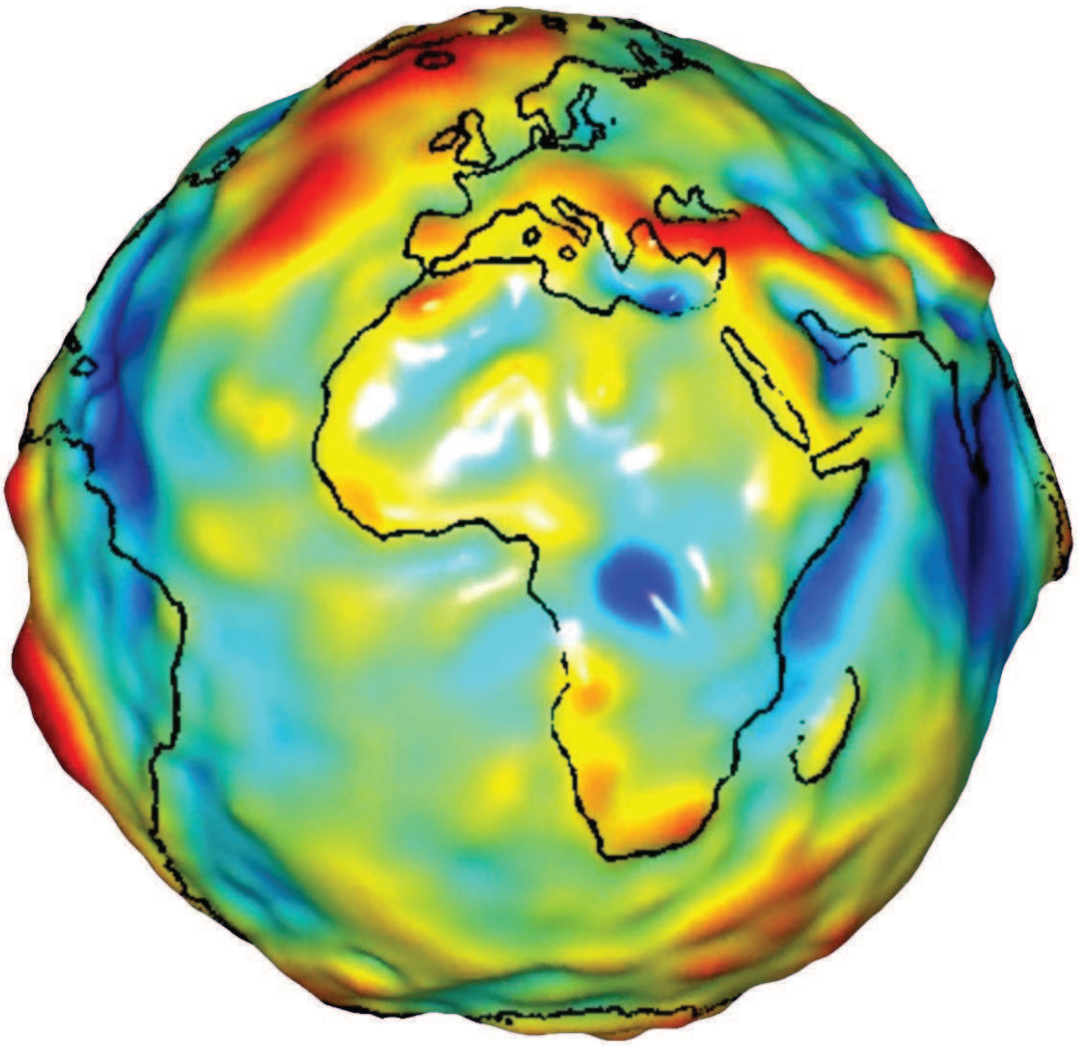

Figure 2.1: GRACE geopotential differences from smooth spherical Earth [1].

In addition to the geopotential, Earth orbiting satellites also experience atmospheric drag, solar radiation pressure and other effects depending on their orbital altitude. For low altitude satellites (below $\sim 350 - 400$ km) atmospheric drag is the dominant perturbation. As the orbital altitude nears Geosynchronous Orbit (GEO) the effects of the gravity field drop off and effects from solar radiation pressure increase. Between these two regions is where the geopotential dominates and where this author seeks to apply the KAM theorem.

Using the KAM theorem to model satellite motion, based on real orbital data, takes into account all of the geopotential effects on the satellite. This is a huge advantage over current methods of orbit determination and prediction which typically use only a subset of the full geopotential. Since all of the geopotential terms are included in a KAM torus defined by the analysis of on orbit data, one should be able to predict more accurately and for longer periods of time than with current methods.

Including the whole of the geopotential in the orbit solution may also allow for modeling of other perturbations. Small changes in drag on the satellite, effects from the Moon, Sun and other celestial bodies may be masked or partially masked by the effects of the geopotential, especially when the effects are on the order of the smallest terms in the geopotential. Once the geopotential is removed it may be possible to more accurately study and model such effects.

2.7 Summary

Modern methods of orbit determination and prediction are hindered by not including all of the terms of the geopotential when integrating the orbit, which leads to errors in the accuracy that build as the period of the integration is increased. The KAM theorem may provide a better method, using actual position data for the analysis to find the fundamental frequencies and the corresponding coefficients. This work attempts to apply KAM theorem to the GRACE and Jason-1 orbits, to show that the orbits could be fit to tori for the purpose of modeling and prediction.

III. Method

This chapter begins with a discussion of the satellites and corresponding data. The fundamental frequencies are defined, followed by a discussion of the algorithm used to find the frequencies from the data. Finally, the construction of the torus is explained, along with how the torus is compared to the original data to understand the accuracy of defining the orbit with this method.

3.1 Data

The GRACE data files were obtained from the Physical Oceanography Distributed Active Archive Center (PO.DAAC) at NASA's Jet Propulsion Laboratory. The positions are obtained from the onboard GPS receivers; they are given in the ECEF coordinate frame at 60 second intervals and are accurate to within a few centimeters [16]. The data files also contain position errors, velocities, velocity errors, data validation fields and other fields that are not required for this analysis [4]. A MATLAB® script was written to extract the x, y, and z positions from the data files.

The Jason-1 data files were obtained from NASA's Goddard Space Flight Center (GSFC). The positions are determined from a combination of the SLR and DORIS tracking of the satellite; they are given in the ECEF coordinate frame at 60 second intervals and are accurate to within 3-4 cm [3]. The data files contain 10-day intervals that correspond to the 10-day repeat cycle of the orbit. To ensure enough data was available for the analysis, three repeat cycles were used. Cycles 133-135 were chosen because they followed a maneuver; this was done to reduce the likelihood that a maneuver would occur during the period of analysis. Again, the data files contained more information than was needed, so a MATLAB® script was written to extract the x, y, and z positions from the data files.

The position data sets for both GRACE and Jason-1 are on the order of $\approx 100,000$ meters and are separated by 60 seconds. This author uses the dimensionless quantities of Distance Units (DU) and Time Units (TU) during analysis, which

reduces the data to on the order of ≈ 1.2 DU.

$$1\ DU = 6378136.3\ m \tag{3.1}$$

$$1\ TU = 806.810988\ s \tag{3.2}$$

In addition to reducing the magnitudes of the position data, the choice of DUs and TUs results in the radius of Earth, $R_\oplus$, and the gravitational parameter, μ, being equal to 1. This simplifies the calculation of the estimate frequencies in Equations (3.3)-(3.5) below.

3.2 Fundamental Frequencies

An Earth orbiting satellite will have three fundamental frequencies: the anomalistic frequency, the Earth's rotation rate plus the nodal regression rate, and the apsidal regression rate. These frequencies determine the time is takes for the satellite orbit to traverse the dimensions of the torus. These frequencies are approximated by Equations (3.3)-(3.5), which include only the J_2 effects on the mean motion, the right ascension of the ascending node, and the argument of perigee [17].

$$\tilde{\omega}_1 \approx \sqrt{\frac{\mu}{a^3}}\left\{1 - \frac{3J_2R_\oplus^2}{2a^2(1-e^2)^{3/2}}\left(\frac{3}{2}\sin^2 i - 1\right)\right\} \tag{3.3}$$

$$\tilde{\omega}_2 \approx \omega_\oplus + \frac{3\sqrt{\mu}J_2R_\oplus^2}{2a(7/2)(1-e^2)^2}\cos i \tag{3.4}$$

$$\tilde{\omega}_3 \approx -\frac{3\sqrt{\mu}J_2R_\oplus^2}{2a^{7/2}(1-e^2)^2}\left(\frac{5}{2}\sin^2 i - 2\right) \tag{3.5}$$

The total time it takes for a satellite to traverse the entire torus is dependent on the smallest frequency. It gives the toroidal period as

$$T_{KAM} = \frac{2\pi}{\omega_3}. \tag{3.6}$$

3.3 Frequency Determination Algorithm

Since the data used in this analysis covers a finite period of time, it seems natural to use a finite time Fourier transform method of the form in Equation 3.7. In this work, the function $f(t)$ is the position coordinates for the orbit.

$$\begin{aligned}\mathcal{F}(\omega) &= \frac{1}{2T}\int_{-T}^{T} f(t)e^{-\omega it}\chi(t)dt \\ &= \frac{1}{T}\int_{0}^{T} f(t)e^{-\omega it}\chi(t)dt - \frac{1}{T}\int_{0}^{-T} f(t)e^{-\omega it}\chi(t)dt\end{aligned} \tag{3.7}$$

The Fourier transform algorithm used in this work is based on Laskar's [10–12] Numerical Algorithm of the Fundamental Frequency (NAFF), which has been shown to identify the frequencies of a quasiperiodic function to a higher precision than a simple Fast Fourier Transform (FFT). An FFT typically assumes the function has a period of 2τ over a range of $[-\tau : \tau]$, with an accuracy proportional to $1/\tau$; Laskar's NAFF does not make this assumption and, with the use of a window function, χ, converges on the frequencies with an accuracy proportional to $1/\tau^4$. The NAFF finds the frequency by iterating over Equation (3.8).

$$\phi(\omega) = \frac{1}{2}\int_{-\tau}^{\tau} f(t)e^{-i\omega t}\chi(t/\tau)dt \tag{3.8}$$

The Hanning window function is used in this analysis and is given by Equation (3.9).

$$\chi(t/\tau) = 1 + \cos\left(\frac{\pi t}{\tau}\right) \tag{3.9}$$

The approximate frequencies from Equations (3.3) - (3.5) are input into the algorithm, as initial guesses, to reduce the number of iterations. As noted above, the precision of the frequency found is higher than it would be with a simple FFT. However, this doesn't mean that the frequencies are exact, just very close.

It should also be noted that the Hanning window function accelerates the convergence of finding the peak frequency; higher order Hanning functions result in faster convergence, though Laskar shows that the cost-to-benefit drops off after windows of order 3-5 [11]. Higher order functions also result in wider peaks, which leads to more uncertainty in the frequency. This author uses the 2nd order Hanning window function, which seems to work fairly well.

Figure 3.1 shows the results of the Fourier transform of the GRACE data. The

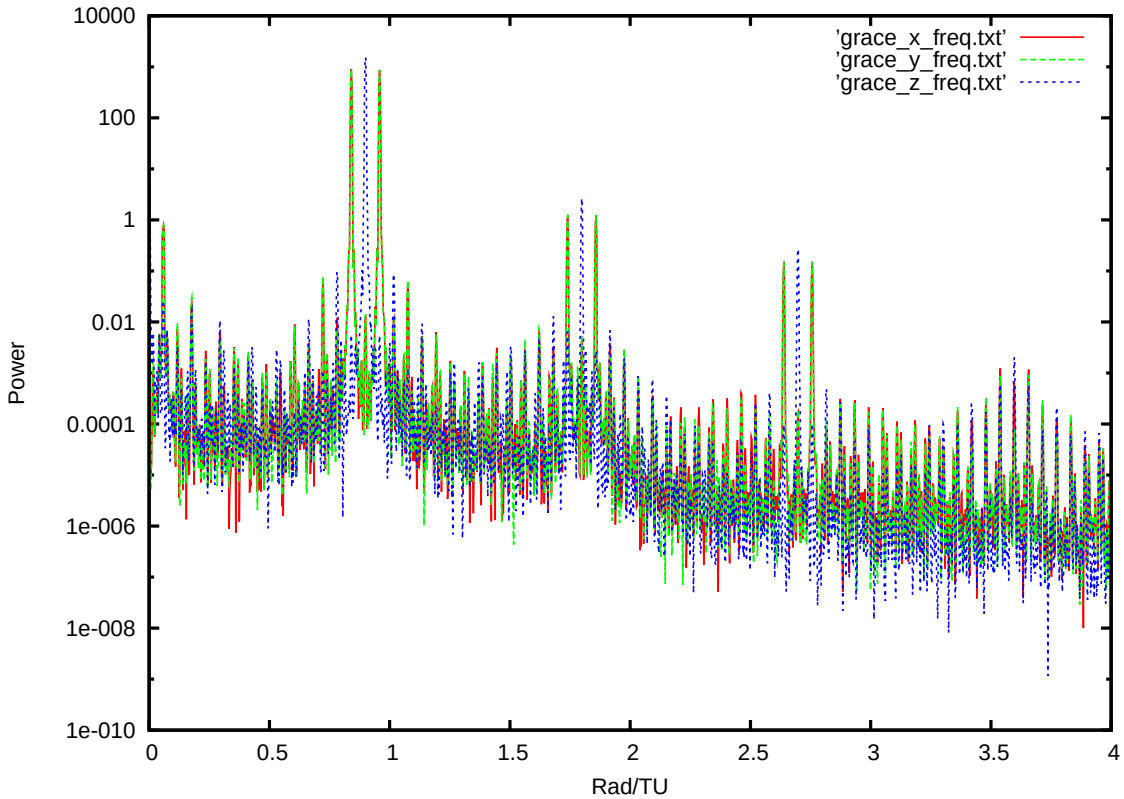

Figure 3.1: PSD plot for the GRACE-A satellite showing how the modified Laskar algorithm finds the frequencies.

triplet structure of the frequencies is due to the fact that ω_2, the combination of $\omega_\oplus$ and the nodal regression rate, is seen in the x and y components of the position, but it does not affect the z. This can be explained by first, noting that all of the components change with the frequency of the orbit, ω_1, but the x and y components also change with $\omega_\oplus$. This is highlighted by the peak in the x and y frequencies, at $\approx 0.0585\ rad/TU$, which corresponds to $\omega_\oplus$, but no such peak exists in the z frequency. Second, the regression of the node is a rotation about the z axis, so it won't show up in the z component of the orbit. The triplet structure of the frequencies is also repeated at equal intervals, which correspond to integer multiples of the orbital frequency, $n\omega_1$. The smaller peaks that flank each large peak are higher order combinations of $n\omega_1 \pm m\omega_2$, where n and m denote integer multiples of the frequencies [15].

The width of the peaks is partially a consequence of the Hanning window and partially a consequence of the finite span of data. Using a larger span of data would reduce the width of the peaks, possibly resulting in more accurate identification of the frequencies. However, the issue that one encounters when analyzing longer periods of on orbit satellite data, is maneuvering. If a torus were already created for an orbit, a maneuver would change the frequencies, the series coefficients, or both, which would require the torus to be recalculated. A maneuver during the analysis of the data could also change the frequencies, resulting in the apparent identification of multiple peaks for each frequency, which would invalidate the analysis.

3.4 The KAM Torus

After the frequencies are identified, the torus can be formed from the fundamental frequencies and the Fourier coefficients. The Fourier coefficients are defined for a single frequency line in [20] as,

$$C = 2\Re A(\omega), \qquad S = 2\Im A(\omega) \tag{3.10}$$

where $A(\omega)$ is the peak amplitude of the frequency multiples found during the Fourier transform analysis. With the frequencies and the coefficients, the coordinates of the KAM torus can be calculated by Equation (3.11); j is the series limit of the coefficients, $\vec{j}$ is a summation vector, and $\vec{\omega}$ is the vector of torus basis frequencies [20].

$$q(t) = C_0 + \sum_j \{C_j \cos(\vec{j} \cdot \vec{\omega} t) + S_j \sin(\vec{j} \cdot \vec{\omega} t)\} \tag{3.11}$$

In this work, a series limit of 10 is used when calculating the Fourier coefficients; this means the coefficients are defined for the frequency harmonics up to $10\omega_1 \pm 10\omega_2$. The constant term C_0 is found from the initial conditions.

Using a known starting position, the positions for any point in the future (or past) can then be calculated and compared to the real data to get the residuals and determine how well the torus approximates the orbit. The torus can have errors in both the frequencies and the Fourier series coefficients, but they show up in distinct and different ways. If there are small errors in the frequencies, they will show up as linear error growth over time. The coefficients define the shape and position of the torus in space, so errors show up in the torus as either a shift from where it should be in space, or in a shape difference from that of the *true* torus.

3.5 Summary

The fundamental frequencies for the GRACE and Jason-1 orbits are found from the modified Laskar algorithm analysis of the precise orbital position data. The Fourier coefficients are then calculated to complete the definition of the KAM tori for each satellite, allowing the orbit to be modeled. The positions are then calculated from the torus and compared to the real position data to determine how well the torus models the orbit.

IV. Results and Findings

This chapter shows that discrete frequencies exist for both the GRACE and Jason-1 satellites. These are then used to create the tori. The tori are used to predict the positions of the satellites and compared to the real orbital data.

4.1 GRACE

This section will cover the frequency estimates for the GRACE-A satellite, followed by the frequencies found using the modified Laskar algorithm. Finally, the torus is compared with the real orbital data.

4.1.1 Frequency Estimates. The estimates for the GRACE frequencies are calculated from Equations (3.3)-(3.5) and are given in Equations (4.1)-(4.3). The values used for calculating the frequencies are given as $a \approx 6843000\ m$, $\mu = 3986004.415E{+}8\ m^3/s^2$, $R_\oplus = 6378136.3\ m$, $i \approx 89°$, $e \approx .0017$, $J_2 = 4.84165339915E{-}4$, and $\omega_\oplus = 7.292115857916E-5\ rad/s$.

$$\begin{aligned} \tilde{\omega}_1 &= 0.899567967941131\ rad/TU \\ &= 1.114967418186E-3\ rad/s \end{aligned} \tag{4.1}$$

$$\begin{aligned} \tilde{\omega}_2 &= 5.8843500509237E-2\ rad/TU \\ &= 7.2933439658E-5\ rad/s \end{aligned} \tag{4.2}$$

$$\begin{aligned} \tilde{\omega}_3 &= 2.83439973794E-4\ rad/TU \\ &= 3.51309014E-7\ rad/s \end{aligned} \tag{4.3}$$

4.1.2 Laskar Frequency Output. The Laskar algorithm only identified the first two frequencies for the GRACE orbit; a value for the third frequency was given, but it was on the order of 10^{-30}, which is effectively zero and assumed to be erroneous.

This is not altogether surprising, since the orbit is very circular, $e \approx .0017465$. This problem occurs for two reasons. First, based on the approximate frequency from equation (4.3), above, we expect the period of a torus for this orbit to be ≈ 207 days. Only 31 days worth of data were used (1-31 Mar 08), so the perigee only moved $\approx .721\ rad$; this makes it difficult to see the movement of the perigee, given the amount of data used. Second, as mentioned in Section 3.3, the peak that identifies the frequency has a width. Since the frequency is already close to zero, the width of the peak identified for the smallest frequency may cross zero, which leads to the error.

The first two frequencies are found to be very close to the approximate frequencies given by Equations (4.1) and (4.2).

$$\omega_1 = 0.899330102615437\ rad/TU \tag{4.4}$$

$$\omega_2 = 5.890847214269741E-2\ rad/TU \tag{4.5}$$

Figures 4.1-4.4 are Power Spectral Density (PSD) plots for the GRACE-A data. The largest peak in Figure 4.1 corresponds to ω_1 and appears in the analysis of the z component because it is unaffected by the Earth's rotation and nodal regression rates. Alternatively, x and y are affected by the Earth's rotation and the nodal regression and so, the largest peaks in Figure 4.2 and Figure 4.3 come from $\omega_1 \pm \omega_2$.

Figure 4.4 has all three components plotted to show how the peaks in the x and y components straddle the z peak. The smaller frequency range displayed, also shows the width of the peaks more clearly than Figures 4.1 - 4.3. As discussed in Section 3.3, the width of the peaks is a source of error in the frequencies. This may in fact be the reason ω_3 was not identified. In the z frequency there is a spike right at zero. It is possible this spike corresponds to ω_3, but due to the width the top of the peak cannot be identified, which makes it impossible to find the frequency. Further analysis is required to confirm this hypothesis.

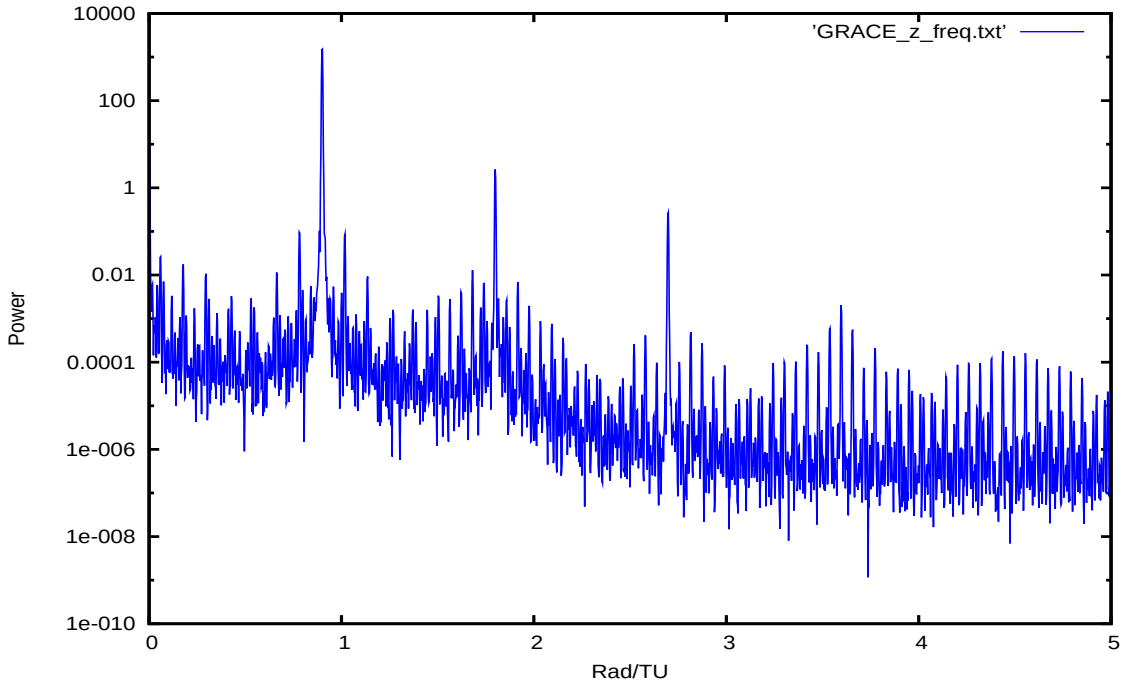

Figure 4.1: z frequency PSD plot for the GRACE-A satellite.

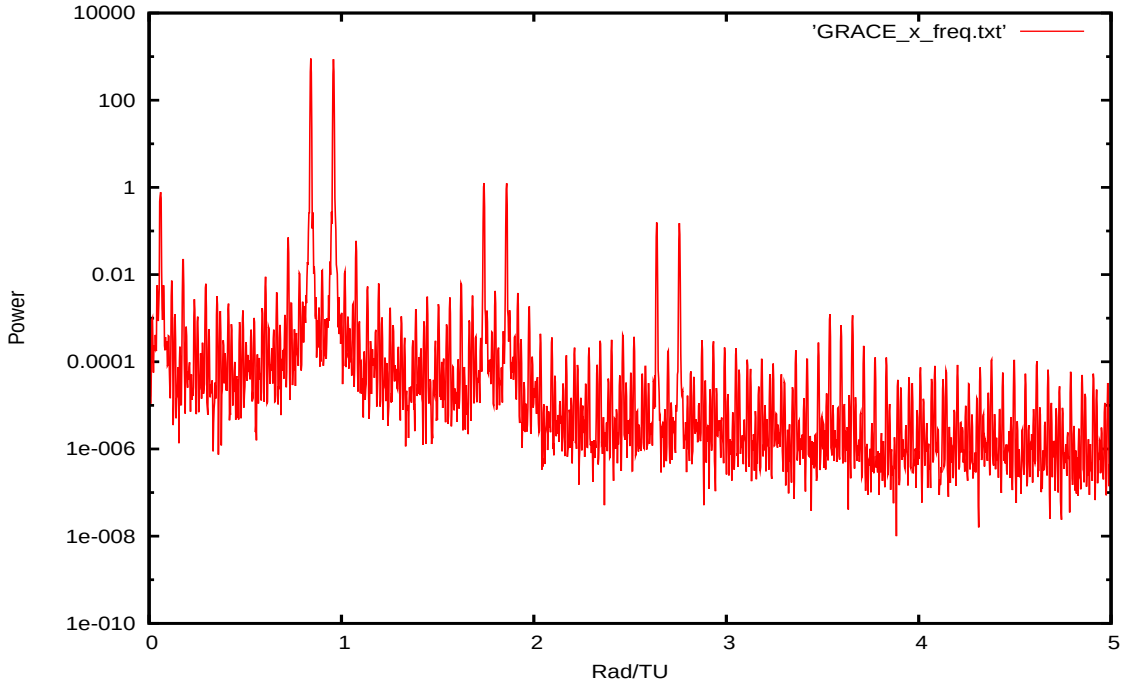

Figure 4.2: x frequency PSD plot for the GRACE-A satellite.

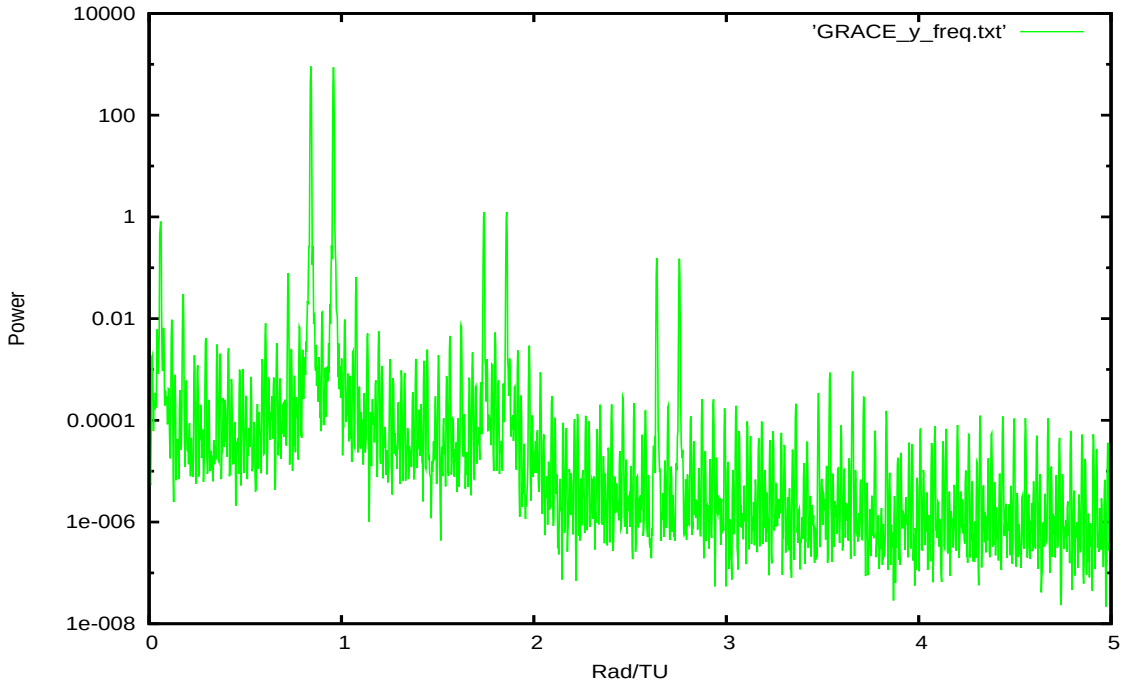

Figure 4.3: y frequency PSD plot for the GRACE-A satellite.

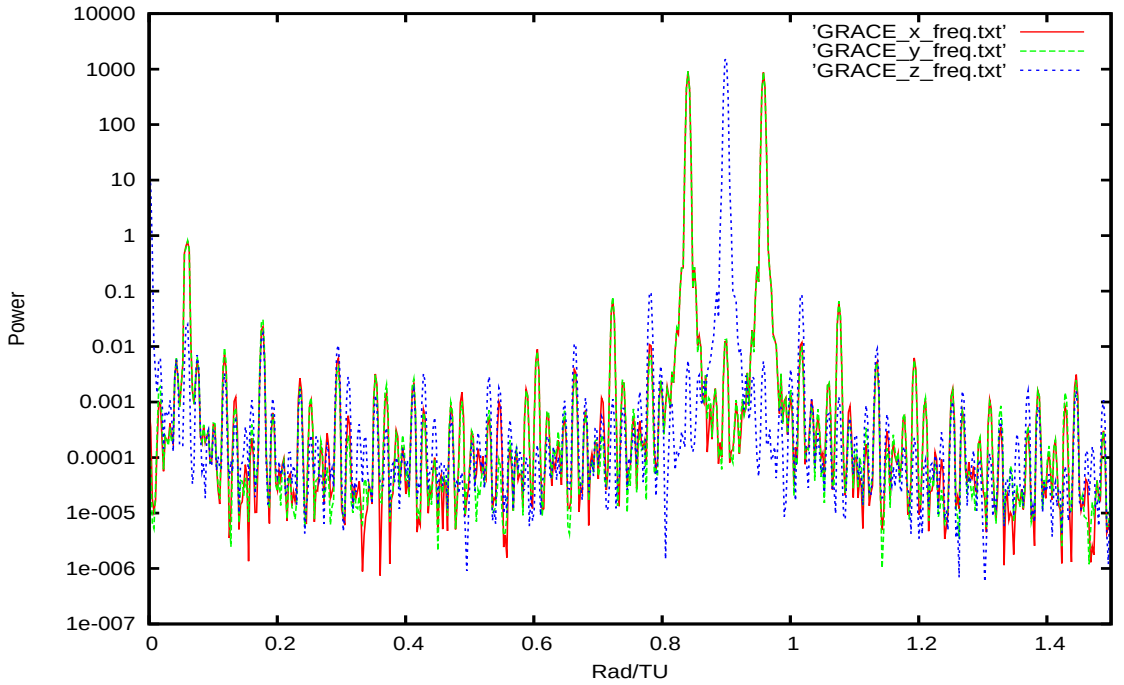

Figure 4.4: GRACE-A PSD plot highlighting the triplet structure of the frequencies.

4.1.3 Comparing KAM to Real Data. After the frequencies were identified by the Laskar algorithm, the torus is formed and compared to the real data, and the residuals were calculated. The initial residuals, which are displayed in Figure 4.5, are nearly zero at the initial conditions, $t = 0$. However, frequency errors are present in both frequencies as evidenced by the error growth as t goes toward $\pm t_{final}$.

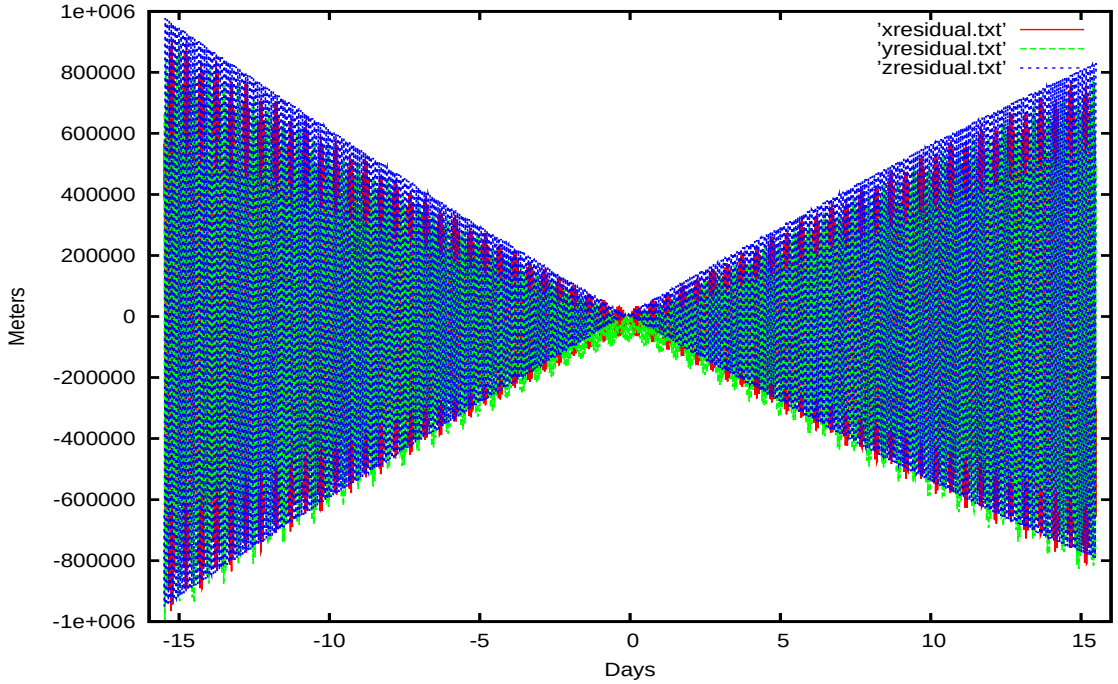

Figure 4.5: This shows the residual growth over time using the frequencies found from the Laskar algorithm.

The frequency errors must be small since they show up as linear error growth; the explanation is given by

$$\begin{aligned} X &= C\cos(\omega_1 + \delta\omega_1)t + S\sin(\omega_1 + \delta\omega_1)t \\ &= C(\cos\omega_1 t\cos\delta\omega_1 t - \sin\omega_1 t\sin\delta\omega_1 t) \\ &\quad + S(\sin\omega_1 t\cos\delta\omega_1 t + \cos\omega_1 t\sin\delta\omega_1 t) \\ &\approx C\cos\omega_1 t - C\delta\omega_1 t\sin\omega_1 t + S\sin\omega_1 t + S\delta\omega_1 t\cos\omega_1 t \end{aligned} \tag{4.6}$$

using standard trigonometric identities and the small angle approximation. The $\delta\omega_1 t$ terms that are left, result in the linear error growth visible in Figure 4.5; the same result can be shown for $\delta\omega_2$.

From the slope of the residual peaks, we can approximate the magnitude of the frequency errors. Since the torus only requires the frequencies and the Fourier coefficients, it is possible to adjust the frequencies, without having to rerun the entire frequency analysis, to try and reduce the error. While adjusting the frequencies, the Fourier coefficients are assumed to be correct and held constant.

The frequency errors for ω_1 and ω_2 were found to be on the order of 10^{-5} rad/TU. Adjusting only ω_1, the frequency error was found to be $\approx 7E-5$ rad/TU. Then, adjusting only ω_2, the frequency error was found to be $\approx 5E-5$ rad/TU; further adjustments were made by making smaller changes to the frequencies. Figure 4.6 shows how the residuals improved after the frequencies were adjusted.

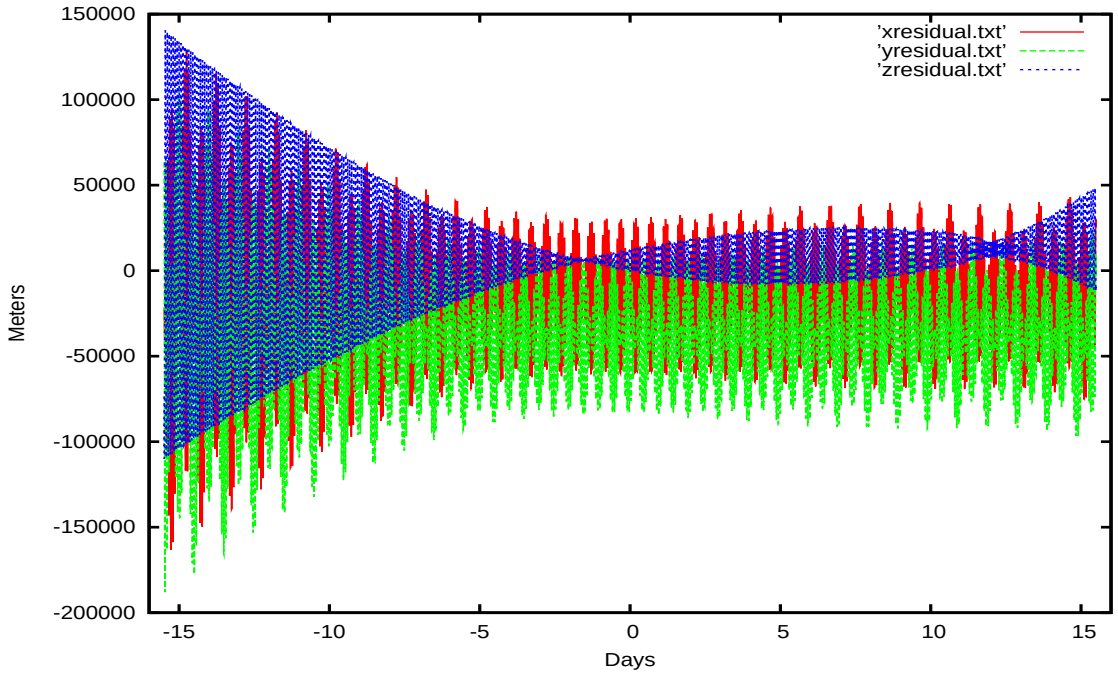

Figure 4.6: Residual improvements with $\delta\omega_1 = 7.4E{-}5$ rad/TU and $\delta\omega_2 = 5.4E-5$ rad/TU.

Further adjustments revealed a limit to the improvement that could be gained by the frequency changes. Figure 4.7 shows the residuals for the frequencies adjust by $\delta\omega_1 = 7.7E-5\ rad/TU$ and $\delta\omega_2 = 5.7E-5\ rad/TU$. Over all, the residuals are much improved over the initial findings. However, the residuals have begun to show a quadratic form in the z component. This is likely due to atmospheric drag, which appears as quadratic changes in the mean anomaly of the orbit [17]. Atmospheric drag is not modeled by the KAM theorem, and must be handled by some other means.

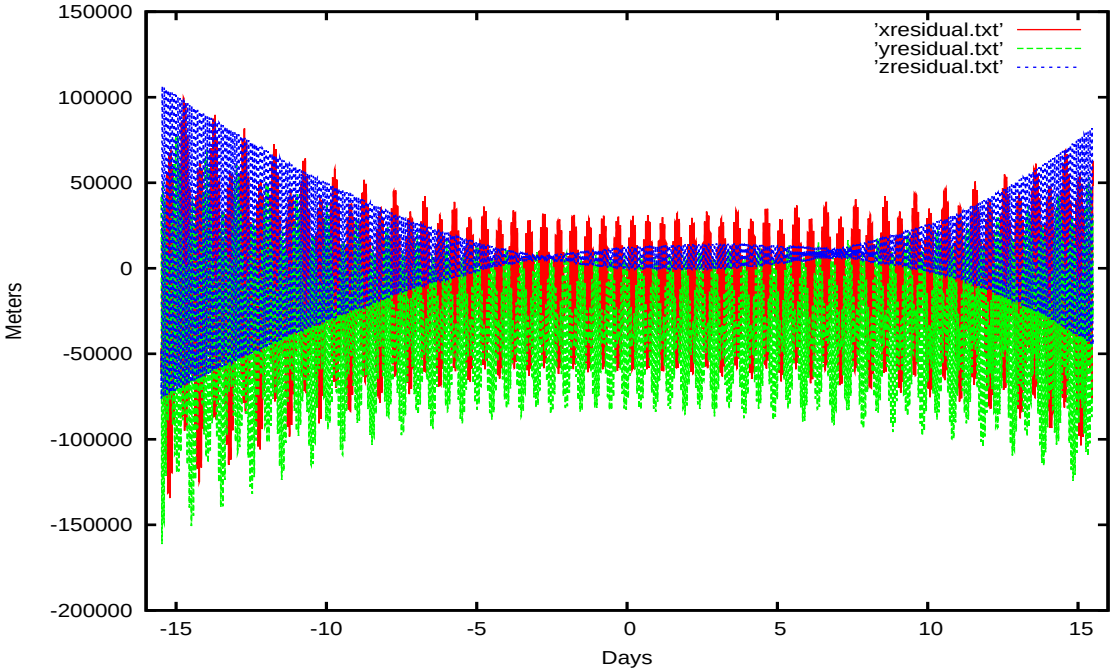

Figure 4.7: Residual improvements with $\delta\omega_1 = 7.7E-5\ rad/TU$ and $\delta\omega_2 = 5.7E-5\ rad/TU$.

Looking closer at the area where the residuals are the smallest, Figure 4.8 shows they are still fairly high. The z coordinate residuals are $\approx 20\ km$, and the x and y coordinate residuals are off by as much as $40-90\ km$.

Some of the error still present in the residuals is due to errors in the coefficients. This is most likely the case with the offset that is present in each of the components; the y component shows the largest offset, but all three have some level of offset. Figure 4.8 also shows a distinct, repeating pattern in the x and y residuals. Looking more

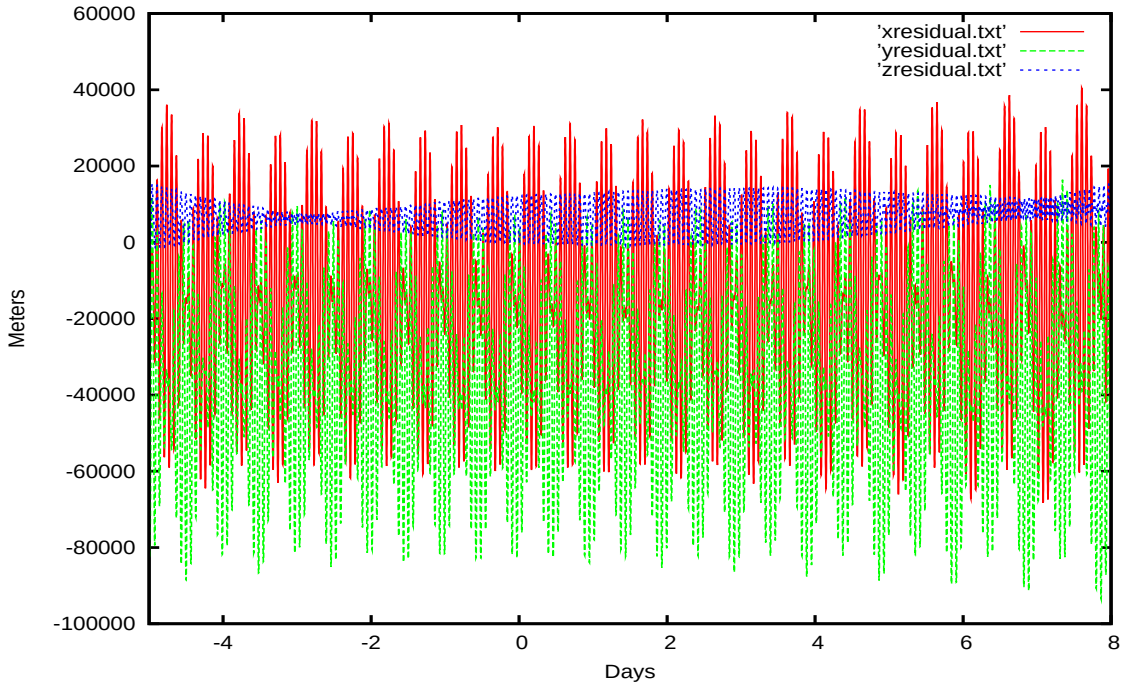

Figure 4.8: This shows the error still present in the region where the frequency adjustment is most effective.

closely at the x residuals, Figure 4.9 shows that the frequency of the peaks is nearly equal to the orbital frequency. There are also consistently 8 peaks in each repetition. This suggests there may be a dominate error in the coefficient defined by the eighth harmonic of ω_1. However, further analysis is needed to confirm this and resolve the issue.

Unfortunately, these remaining errors are too large for the torus to be useful for modeling the orbit. If these errors could be driven down further, through refinement of the torus, it may be possible to model the GRACE orbit with a KAM torus. However, perturbation theory would still be required to account for the effects of atmospheric drag.

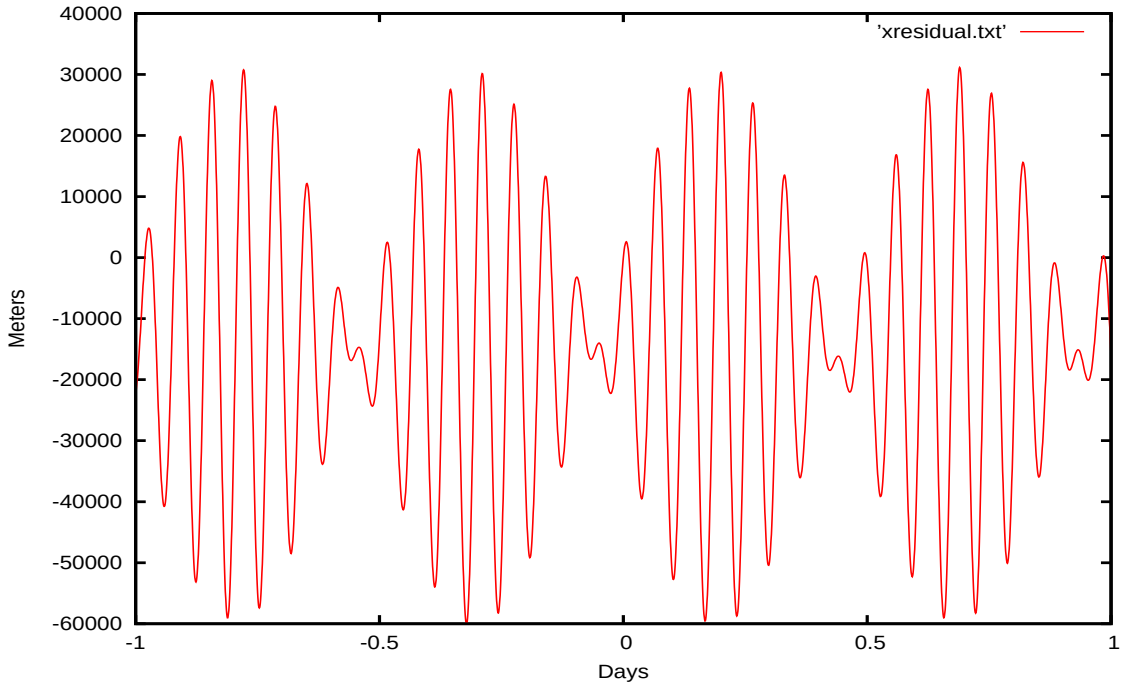

Figure 4.9: Periodic changes in the GRACE x residuals.

4.2 Jason-1

This section will cover the frequency estimates for the Jason-1 satellite, followed by the frequencies found using the modified Laskar algorithm. Finally, the torus will be compared with the real orbital data.

4.2.1 Frequency Estimates. The estimates for the Jason-1 frequencies are calculated from Equations (3.3)-(3.5) and are given by Equations (4.7)-(4.9). The values used for calculating the frequencies are given as $a = 7715636.3\ m$, $\mu = 3986004.415E+8\ m^3/s^2$, $R_\oplus = 6378136.3\ m$, $i \approx 66°$, $e = .0007465$, $J_2 = 4.84165339915E-4$, and $\omega_\oplus = 7.292115857916E-5\ rad/s$.

$$\begin{aligned} \tilde{\omega}_1 &= 0.751499356368578\ rad/TU \\ &= 9.31560930902E-4\ rad/s \end{aligned} \tag{4.7}$$

$$\tilde{\omega}_2 = 5.8985058639173E-2\ rad/TU \tag{4.8}$$
$$= 7.3108893552E-5\ rad/s$$

$$\tilde{\omega}_3 = 3.2735245545E-5\ rad/TU \tag{4.9}$$
$$= 4.0573624E-8\ rad/s$$

4.2.2 Laskar Frequency Output. The Laskar algorithm only identified the first two frequencies for the Jason-1 orbit; a value for the third frequency was given, but it was on the order of 10^{-28}, which is effectively zero and considered erroneous. This is not altogether surprising, since the orbit is very circular, $e = .0007465$. This problem occurs for two reasons. First, based on the approximate frequency from equation (4.9), above, we expect the period of a torus for this orbit to be ≈ 5 years. Only $\approx$ 30 days worth of data were used, so the perigee only moved $\approx .103\ rad$; this means it would be difficult to see the movement of the perigee in the period analyzed. Second, as mentioned in section 3.3, the peak that identifies the frequency has a width. Since the frequency is already close to zero, the width of the peak for the smallest frequency may cross zero, which leads to the error.

The first two frequencies are found to be very close to the approximate frequencies given by equations (4.7) and (4.8).

$$\omega_1 = 0.751485615955426\ rad/TU \tag{4.10}$$

$$\omega_2 = 5.915352315796121E-2\ rad/TU \tag{4.11}$$

Figures 4.10-4.13 are PSD plots for the Jason-1 data. The largest peak in Figure 4.10 corresponds to ω_1. As discussed above, it appears in the analysis of the z component because it is unaffected by the Earth's rotation and nodal regression rates. Again, x and y are affected by the Earth's rotation and the nodal regression

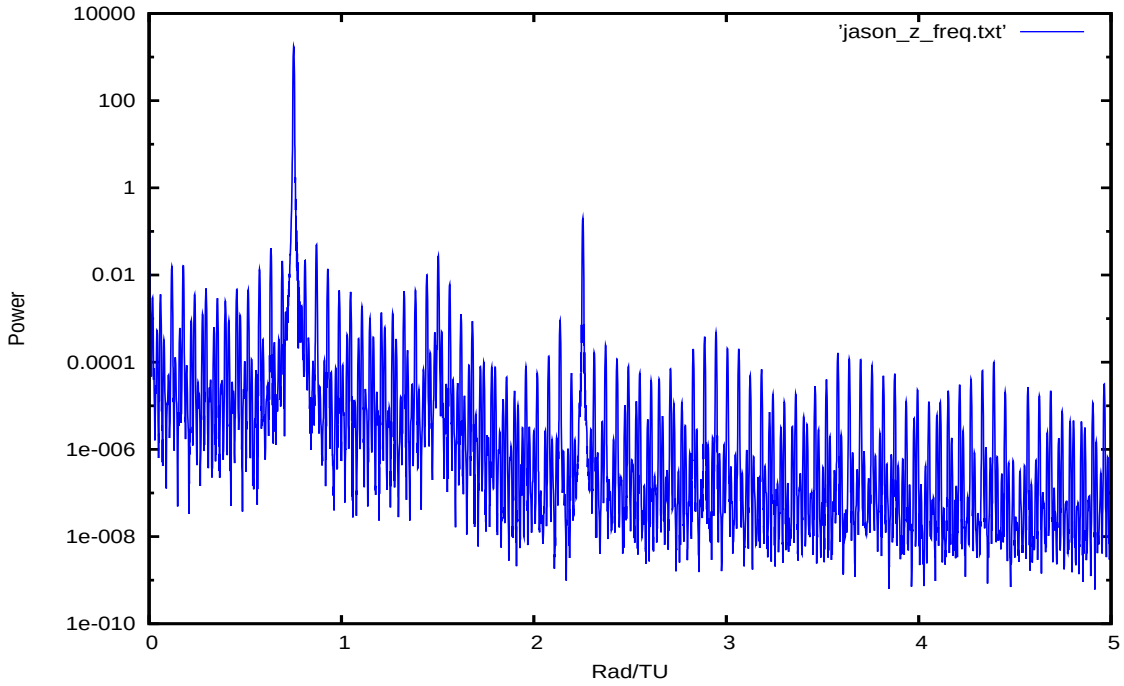

Figure 4.10: The z frequency PSD plot for the Jason-1 satellite.

and the largest peaks in Figure 4.11 and Figure 4.12 come from $\omega_1 \pm \omega_2$. Figure 4.13 has all three components plotted to show how the peaks in the x and y components straddle the z peak.

Another result to note in Figures 4.10-4.12 is the magnitudes of the peaks. In Fourier analysis of quasiperiodic systems, one expects that the power will fall off with increasing integer multiples of the frequencies [15], e.g. $A(\omega_1) > A(2\omega_1) > A(3\omega_1)$. This is not the case for Jason-1. Looking specifically at Figure 4.10, it can be seen that the power of the peak for $3\omega_1$ is less than the peak for ω_1, as expected, but larger than the power of the peak for $2\omega_1$, which is contrary to what we expect. This suggests there may be an error in the coefficient calculated for the $2\omega_1$ frequency line, which will show up as errors in the residuals when the torus is compared to the real data.

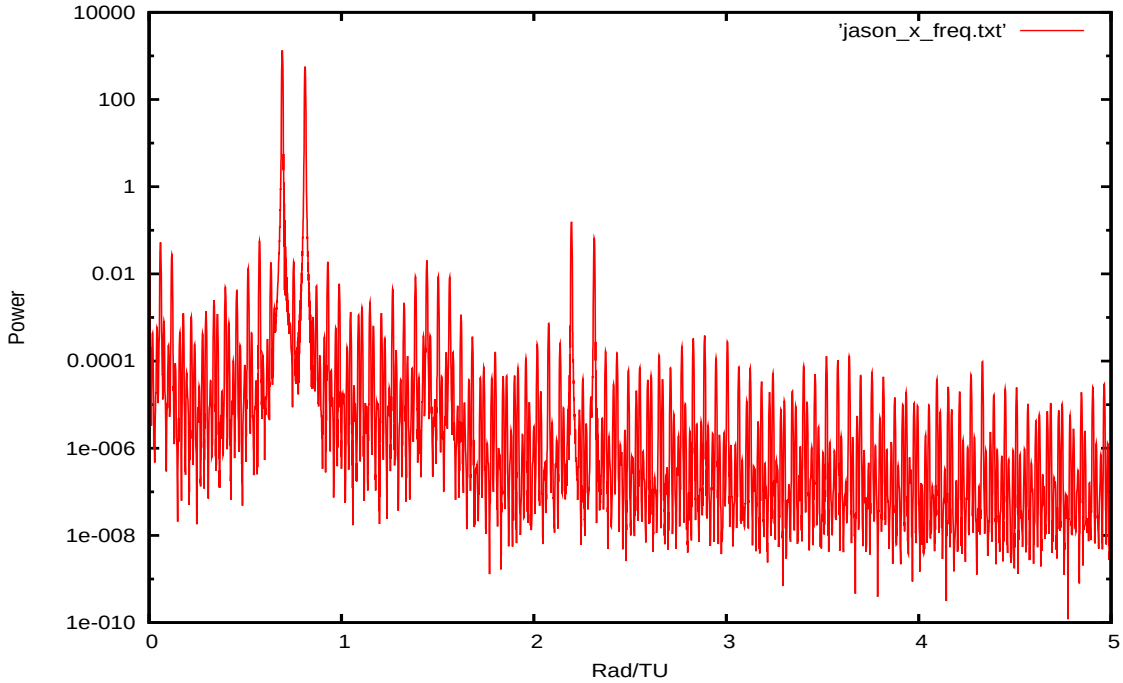

Figure 4.11: The x frequency PSD plot for the Jason-1 satellite.

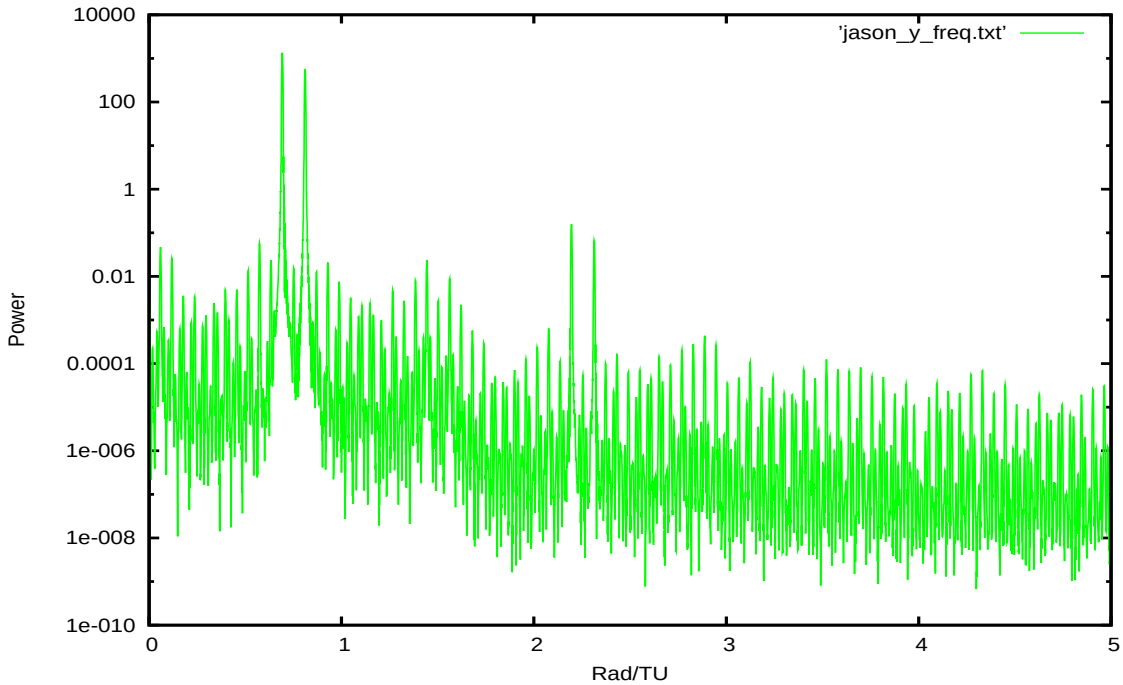

Figure 4.12: The y frequency PSD plot for the Jason-1 satellite.

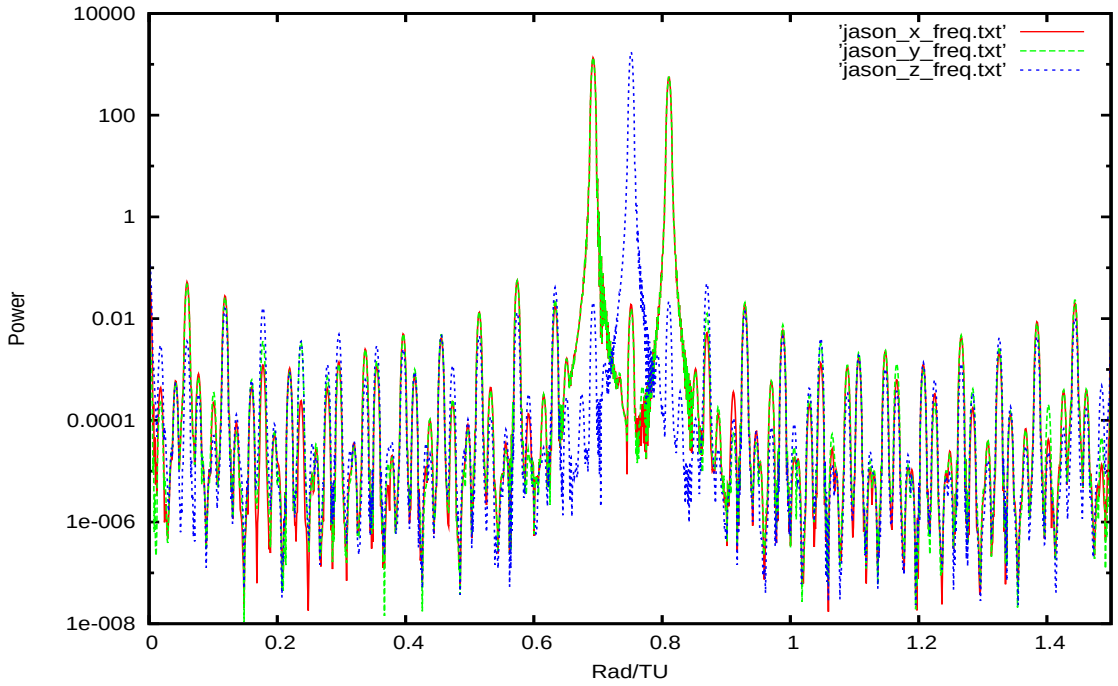

Figure 4.13: Jason-1 PSD plot showing the triplet structure of the frequencies.

4.2.3 Comparing KAM to Real Data. After the frequencies were identified by the Laskar algorithm, the torus is formed and compared to the real data, and the residuals were calculated. The initial residuals, which are displayed in Figure 4.14, are nearly zero at the initial conditions, $t = 0$. However, a frequency error in ω_2 appears as error growth when t goes toward $\pm t_{final}$; the lack of frequency error in ω_1 is shown by the fact that the z residuals remain *near* zero over the entire time span.

The frequency error is small, resulting in linear error growth (see equation (4.6)). From the slope of the residual peaks, we can approximate the magnitude of the frequency error. Since the torus only requires the frequencies and the Fourier coefficients, it is possible to adjust the frequency, without having to rerun the entire frequency analysis, to try and reduce the error. While adjusting the frequency that was in error, the other frequency and the Fourier coefficients are assumed to be correct and held constant.

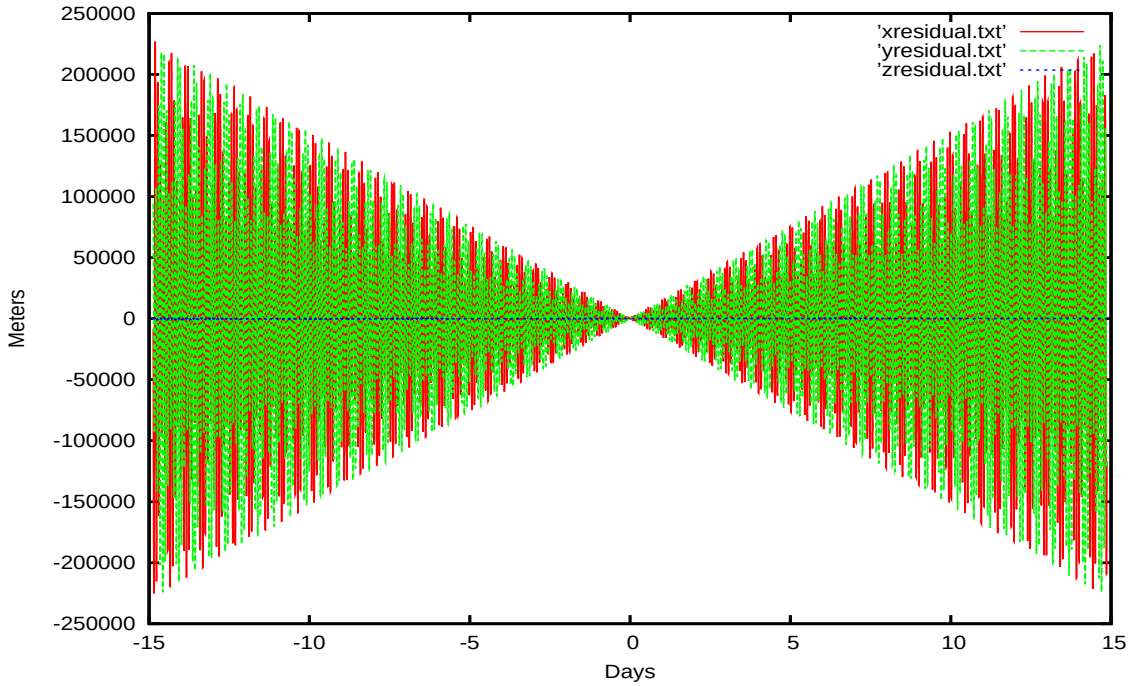

Figure 4.14: This shows the residual growth over time using the frequencies found from the Laskar algorithm.

For Jason-1, the frequency error was found to be on the order of $10^{-5}\ rad/TU$. After some analysis, it was determined that the error was $\approx 1.861E-5\ rad/TU$, with the adjusted frequency given in Equation (4.12).

$$\omega_2 = 5.917213315796121E-2\ rad/TU \tag{4.12}$$

Figure 4.15 shows the residuals after the frequency correction. The root mean square of the residuals is less than 240 meters, and at no point in the period of analysis do the residuals exceed 1 km.

Based on the discussion in Section 4.2.2, a large part of the remaining error is believed to be due to coefficient errors. Figure 4.16 highlights the x residuals for Jason-1, which do not show a periodic repetition over the span of data like that seen in the GRACE data. This suggests that unlike the GRACE results, where it seemed the majority of the coefficient error was due to one harmonic, the Jason-1 residual errors may be due to multiple coefficient errors.

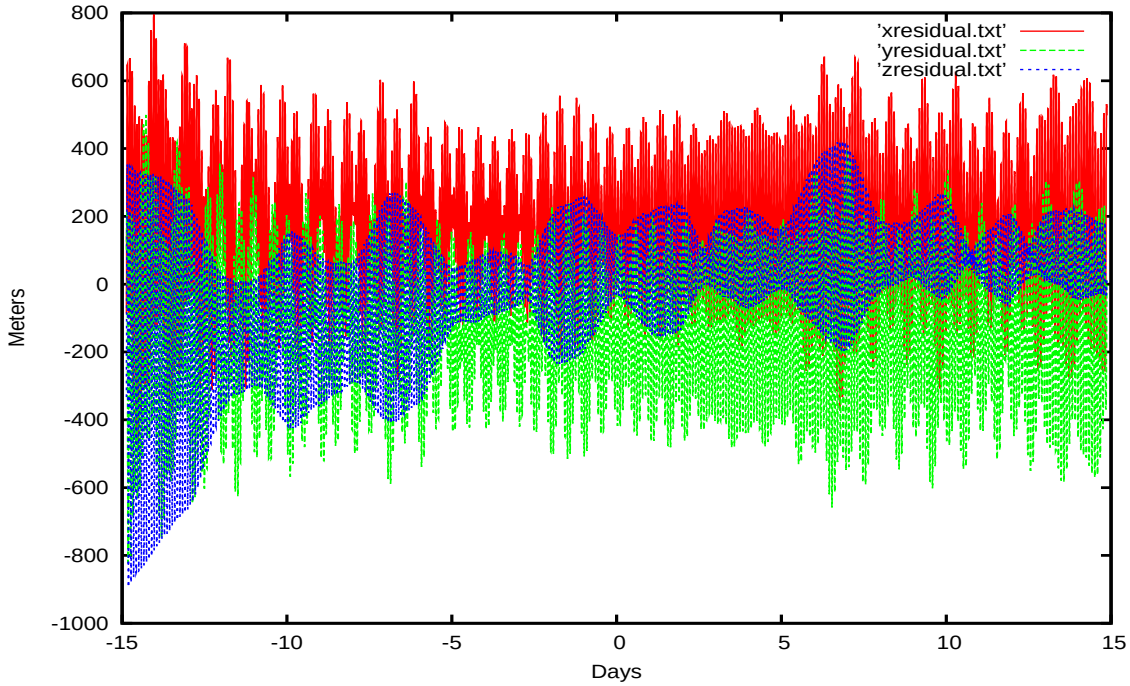

Figure 4.15: This shows the residuals over time after the frequency error was corrected.

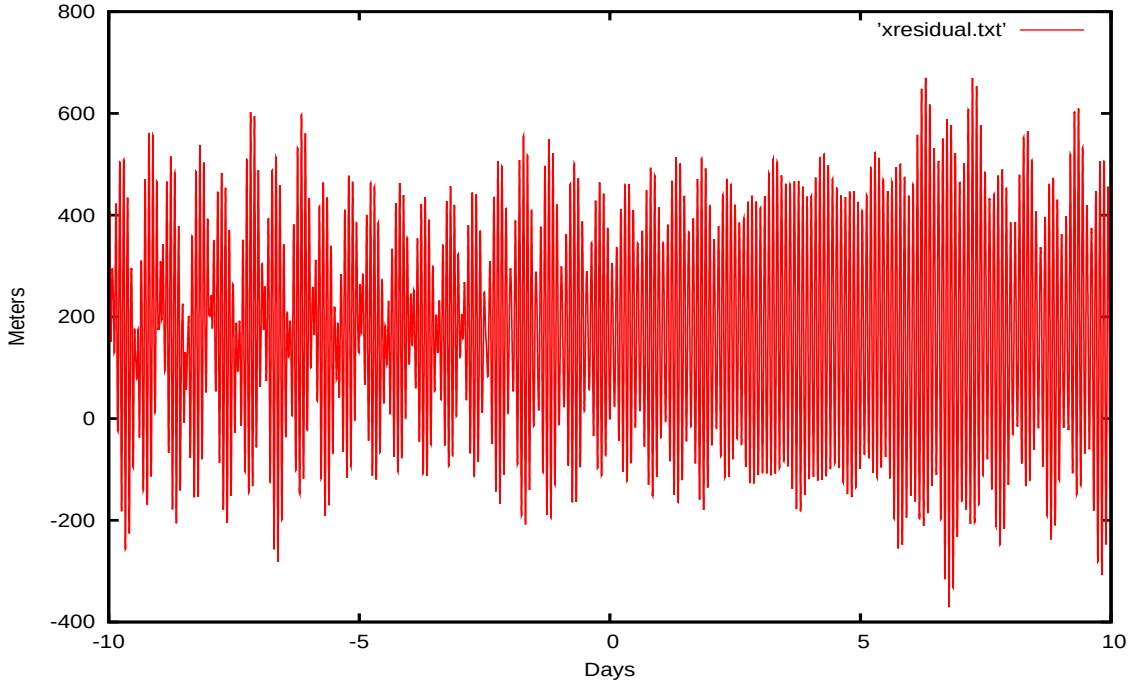

Figure 4.16: The x residuals show no short term pattern.

4.3 Summary of Results

KAM tori were created for both satellites, but after correcting for frequency errors, only the Jason-1 torus was able to produce residuals with a reasonable level of accuracy. The GRACE data produced results indicating that atmospheric drag cannot be ignored, which hinders the ability of KAM theorem to define the orbit without further studies. The Jason-1 torus is promising, but further refinement is needed to justify its use for orbit modeling.

V. Conclusions

This chapter presents the conclusions that are based on the results from Section IV. As with the results, each satellite is discussed individually. Finally, recommendations are made for further study into the applicability of using KAM theorem to define the orbits for GRACE and Jason-1.

5.1 GRACE

The results from Section 4.1 suggest that the GRACE satellites may lie on a torus; however, the effects of atmospheric drag cannot be ignored. There also appear to be errors in the coefficients that must be resolved in order to accurately define the torus. If the coefficient errors can be resolved, it should be possible to define the torus and use perturbation theory to account for the effects of the atmospheric drag; however, further study is required to confirm this.

5.2 Jason-1

The results from Section 4.2 indicate that the Jason-1 satellite does lie on a torus. The comparison of the torus data with the real data shows good agreement, but there is still error that needs to be removed. Analysis of the Fourier coefficients should be able to resolve the errors present.

5.3 Recommendations for Further Study

The methods employed in this work provide a good starting point for defining KAM tori for on orbit satellites. The next step should take the frequencies and Fourier coefficients identified by this method and refine them further, with a fitting algorithm, such as least squares.

The period of validity also needs to be studied. Characterization of how the errors continue to change and grow outside of the period of data used in the analysis is needed. The Jason-1 torus defined in this study could be used for a first analysis of

this problem, but a torus that is further refined, such as with the methods mentioned above, would be more advantageous.

Characterization of the altitude range for the KAM tori should also be done to understand where the non-geopotential perturbations can be ignored. As shown by the GRACE results, lower altitude satellites must deal with the effects of atmospheric drag; similarly, much higher altitude satellites are significantly affected by the Moon, Sun and solar radiation pressure, and must take into account these effects. Understanding where these regions reside will allow for studies into how the perturbations affect the KAM tori and how the effects can be overcome.

Appendix A. Data files

A.1 GRACE

The GRACE data files are extracted from the larger Level-1B (L1B) data files that are available from the PO.DAAC at JPL. The L1B files are produced for each day and can produce a large number of smaller data files. Table A.1 describes the format of the L1B data file containing the positions used in this work.

Table A.1: The NASA code obtained from JPL produces the GNV1B data files containing the following fields [4].

Parameter	**Definition**	**Data Type**	**Byte Length**	**Units**
gps_time	seconds past noon 01-Jan-2000	Integer	4	s
GRACE_id	GRACE satellite identifier	Character	1	N/A
coord_ref	Coordinate reference frame where E = Earth Fixed T = Inertial	Character	1	N/A
xpos	Position, x value (ITRF)	Double Precision	8	m
ypos	Position, y value (ITRF)	Double Precision	8	m
zpos	Position, z value (ITRF)	Double Precision	8	m
xpos_err	Formal error on x position	Double Precision	8	m
ypos_err	Formal error on y position	Double Precision	8	m
zpos_err	Formal error on z position	Double Precision	8	m
xvel	Velocity along x-axis (ITRF)	Double Precision	8	m
yvel	Velocity along y-axis (ITRF)	Double Precision	8	m
zvel	Velocity along z-axis (ITRF)	Double Precision	8	m
xvel_err	Formal error in velocity along x-axis	Double Precision	8	m
yvel_err	Formal error in velocity along y-axis	Double Precision	8	m
zvel_err	Formal error in velocity along z-axis	Double Precision	8	m
qualflg	Data quality flag (LSB = bit 0) bit 0 = Not Defined bit 1 = Not Defined bit 2 = overlap data missing before start midnight bit 3 = overlap data missing after start midnight bit 4 = overlap data missing before end midnight bit 5 = overlap data missing after end midnight bit 6 = Not Defined bit 7 = Not Defined	Unsigned Character	1	N/A

A.2 Jason-1

The Jason-1 data files are available from the GSFC FTP site in the format described in Table A.2. However, to ensure the data is accurate it must be run through the Hermite interpolator, also available from the GSFC FTP site [8]. After the interpolator has been run on the data, it outputs the positions in the ECEF reference frame, as well as velocities, timing data and other information that was not used by this author.

Table A.2: The Hermite interpolator code obtained from NASA ingests the following information, to produce the ECEF position used in this work.

Record	**Item**	**Format**	**Description of Format**
N	1	D22.16	Epoch year, month, day, hour, min satellite time in form YYMMDDhhmm (UTC)
N	2	D22.16	Epoch seconds satellite time (UTC)
N	3	D22.16	Sidereal time - Greenwich hour angle satellite epoch (DEGREES)
N	4	D22.16	Polar motion X (milli arc-seconds)
N	5	D22.16	Polar motion Y (milli arc-seconds)
N	6	D22.16	Epoch time in ET days from Jan 0.0 of the reference year of the arc (days)
N+1	7-9	3D22.16	Satellite Inertial True of Date (ITOD) X,Y,Z elements (meters)
N+1	10-12	3D22.16	Satellite ITOD $\dot{X}$,$\dot{Y}$,$\dot{Z}$ elements (meters/second)
N+2	13-15	3D22.16	Satellite Earth Centered Fixed (ECF) X,Y,Z elements (meters)
N+2	16-18	3D22.16	Satellite ECF $\dot{X}$,$\dot{Y}$,$\dot{Z}$ elements (meters/second)
N+3	19	22I1	Flags indicating orbit mode (0=no, 1=yes) (1) OCCULTATION (0=sun, 1=shadow) Yaw steering events (nominal Beta' example) (2) +ON (15 to 80 DEG BETA') (3) +OFF (0 to 15 DEG BETA') (4) +HIGH OFF (80 to 90 DEG BETA') (5) +RAMP UP (15 to 15.1DEG BETA') (6) +RAMP DOWN (15 to 14.9DEG BETA') (7) +FLIP (+0 to -0 DEG BETA') (8) -ON (-15 to -80 DEG BETA') (9) -OFF (0 to -15 DEG BETA') (10)-HIGH OFF (-80 to -90 DEG BETA') (11)-RAMP UP (-15 to-15.1DEG BETA') (12)-RAMP DOWN (-15 to-14.9DEG BETA') (13)-FLIP (-0 to +0 DEG BETA') (14 - 22) spare
N+3	20	D22.16	Beta' angle (degrees)
N+3	21	D22.16	Yaw angle (degrees)
N+3	22	D22.16	Orbit angle (degrees)
N+3	23	D22.16	Solar array pitch angle (degrees)

Appendix B. Additional GRACE Results

This appendix provides results for the GRACE satellite that were obtained during the analysis. A *brute force* method for changing the frequencies is highlighted here, and was used to arrive at the final results and conclusions presented in main body of this thesis.

Figures B.1-B.3 show the initial GRACE residuals for each component. The error growth in the z component has to be due to a frequency error in ω_1, since ω_2 does not show up in the z component. The error growth in the x and y components may be due to the error in ω_1, or an error in ω_2, or possibly both.

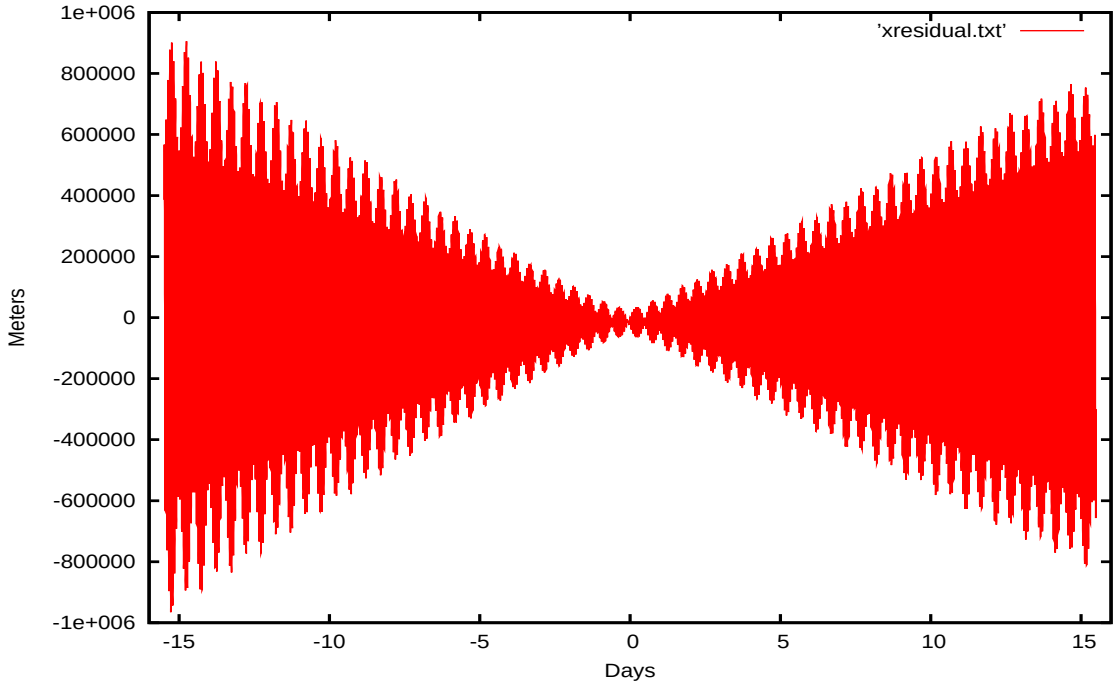

Figure B.1: The residual growth over time in the x component.

Since ω_1 is present in all the components, this frequency was changed first. Examining the slope of the error growth on the z component, the author found the expected error to be on the order of $10^{-5}\ rad/TU$. The z residuals after a change of $1E-5\ rad/TU$ are presented in Figure B.4, and show a small improvement over the initial z residuals presented in Figure B.3. Adjustments were made to reduce the error

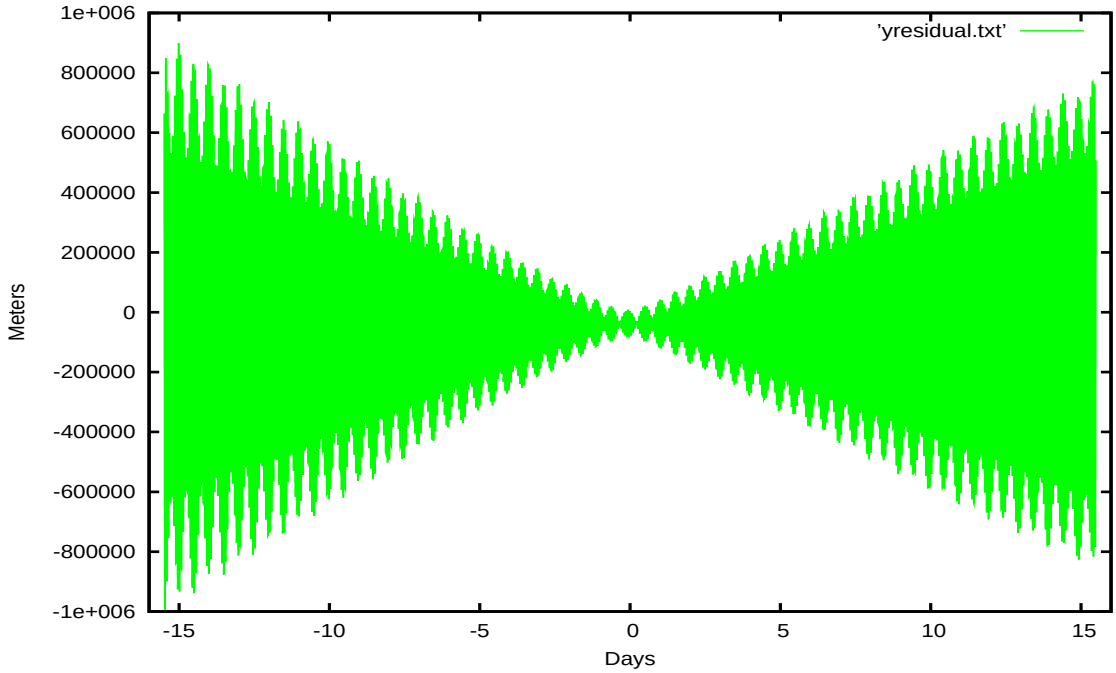

Figure B.2: The residual growth over time in the y component.

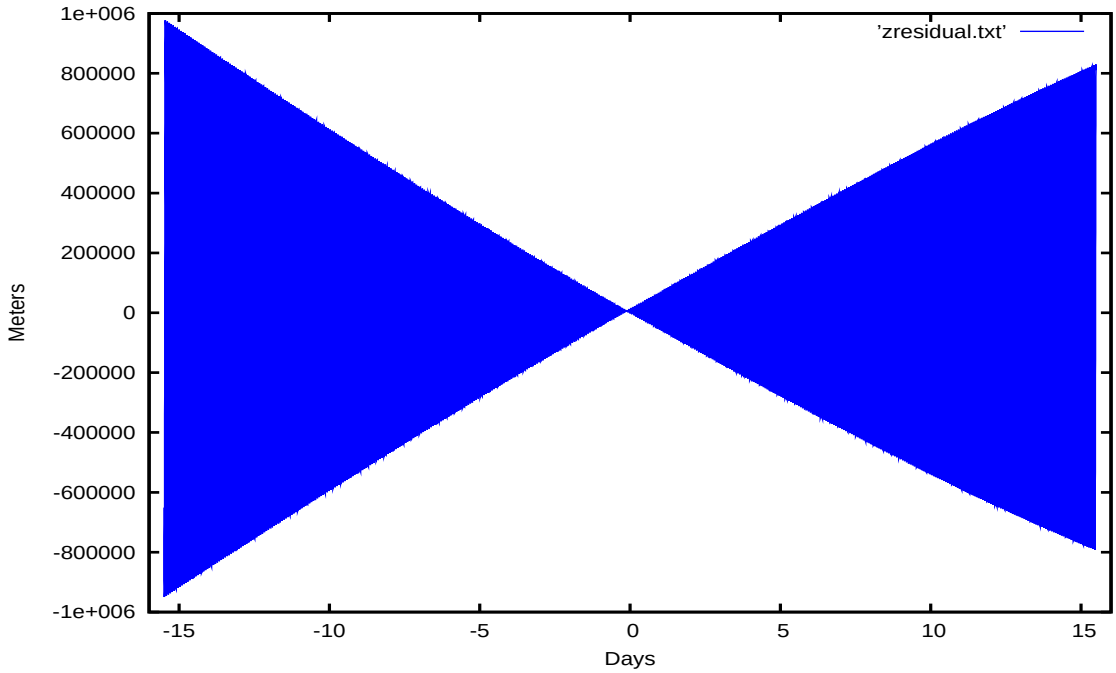

Figure B.3: The residual growth over time in the z component.

growth in z over time, until the frequency adjustment reached $7E{-}5\ rad/TU$. Further adjustments on the order of $10^{-5}\ rad/TU$ resulted in the error growth increasing again. Figure B.5 shows the residuals after the frequency adjustment.

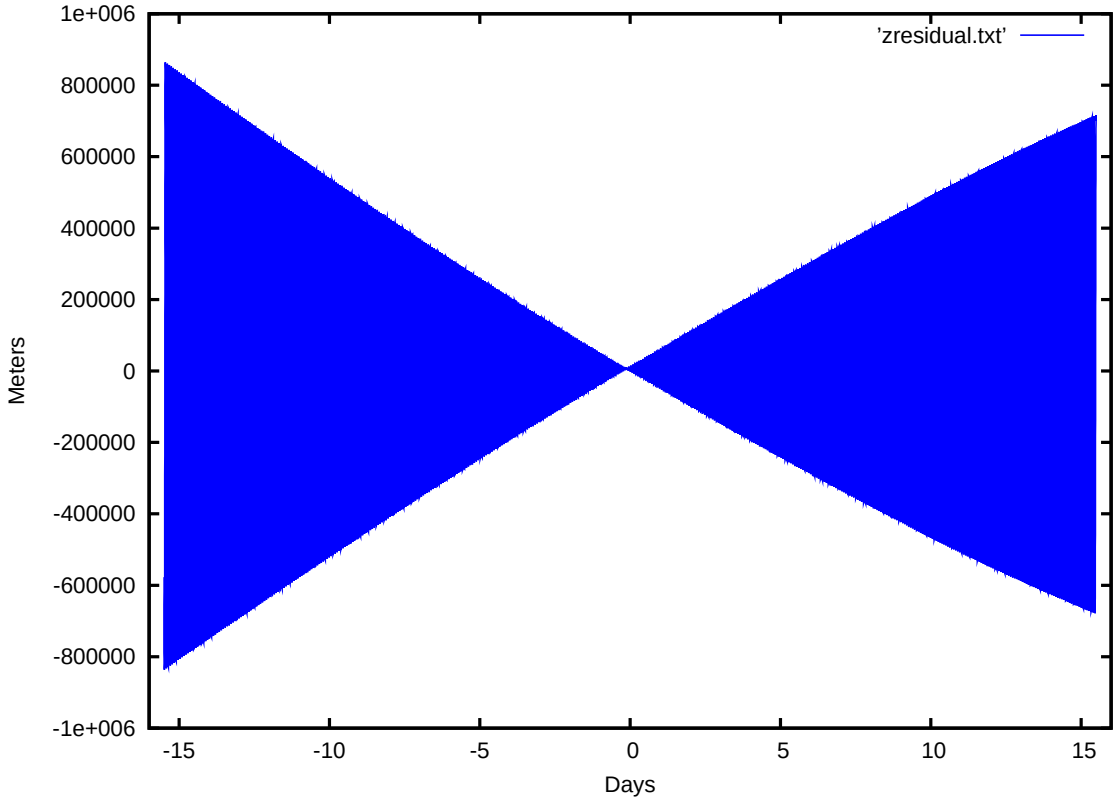

Figure B.4: The residual growth over time in the z component with a frequency adjustment of $\delta\omega_1 = 1Eneg5\ rad/TU$.

Figure B.5 shows the error growth in x and y decreased from those shown in Figures B.1 and B.2. However, the residuals still show a frequency error on the order of $10^{-6}\ rad/TU$. Since the ω_1 frequency error has been partially resolved, the remaining frequency error in x and y must be from errors in ω_2. Following the same method as above, the frequency error was found to be $\approx 5E-6\ rad/TU$. Figure B.6 shows the residuals with the both frequencies adjusted.

An interesting characteristic shows up in the residuals displayed in Figure B.6. The residuals on the left are much greater than the residuals on the right. Finer

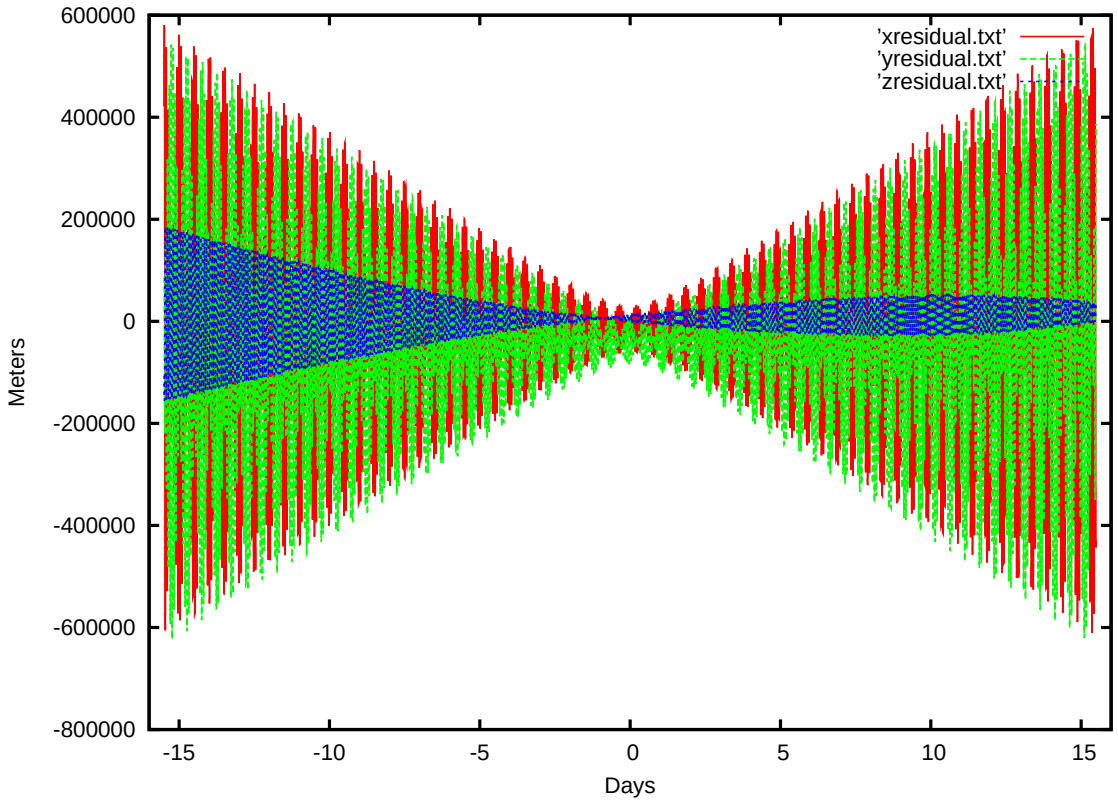

Figure B.5: The GRACE residuals after the frequency change of $\delta\omega_1 = 7Eneg5\ rad/TU$.

adjustments to the frequencies only leads to balancing the *ends* of the residuals, but the overall magnitudes are not greatly reduced. This can be seen in Figure 4.7. The reason the overall residuals cannot be furthered improved is the existence of atmospheric drag on the GRACE satellite. This also accounts for the quadratic shape in the z residuals.

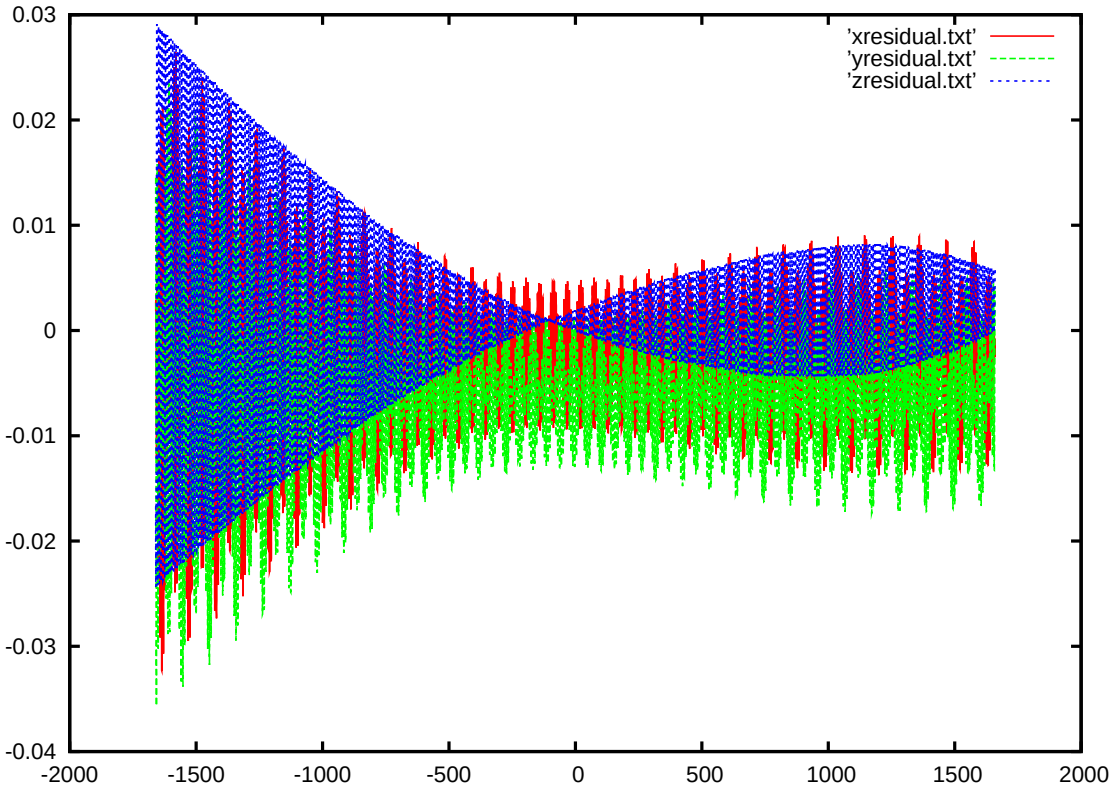

Figure B.6: The GRACE residuals after the frequency changes of $\delta\omega_1 = 7Eneg5 \ rad/TU$ and $\delta\omega_2 = 5Eneg6 \ rad/TU$.

Appendix C. Additional Jason-1 Results

This appendix provides additional results for the Jason-1 satellite that were obtained during the analysis. A *brute force* method for changing the ω_2 frequency is highlighted here.

Figures C.1-C.3 show the difference in the initial x and y residuals and the initial z residuals. Notice that the z residuals are same as those presented in Figure 4.15 without any changes to the frequencies, but the x and y are off significantly. From this, the author knew that the only significant frequency error was in ω_2.

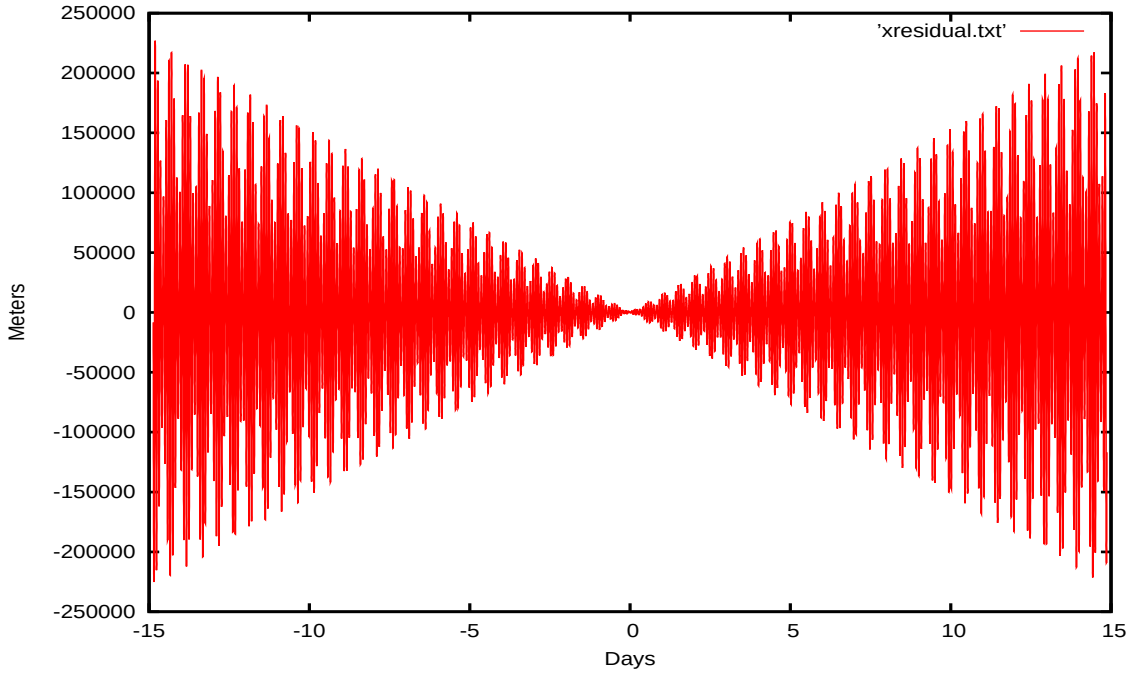

Figure C.1: The residual growth over time in the x component.

The slope of the residual growth in x and y indicates that the error in ω_2 is on the order of 10^{-5}. Figure C.4 shows that adjusting the frequency by $1E-5$ reduced the residuals by about $\frac{1}{2}$. However, the residuals are still off by $\approx$ 100 km. Figure C.5 shows that adjusting the frequency by $2E-5$ reduced the residuals by an order of magnitude.

The goal for this work was to get the residuals to about 1 km. Having already improved the residuals from $\approx$ 200 km down to $\approx$ 15 km, the author assumed that

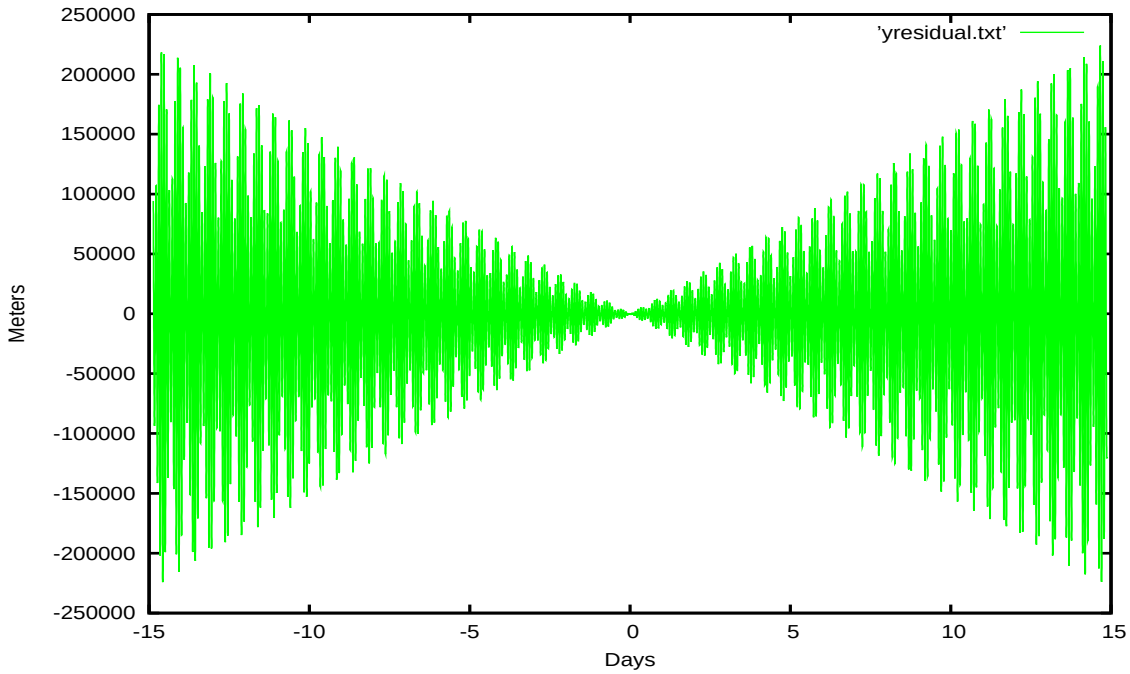

Figure C.2: The residual growth over time in the y component.

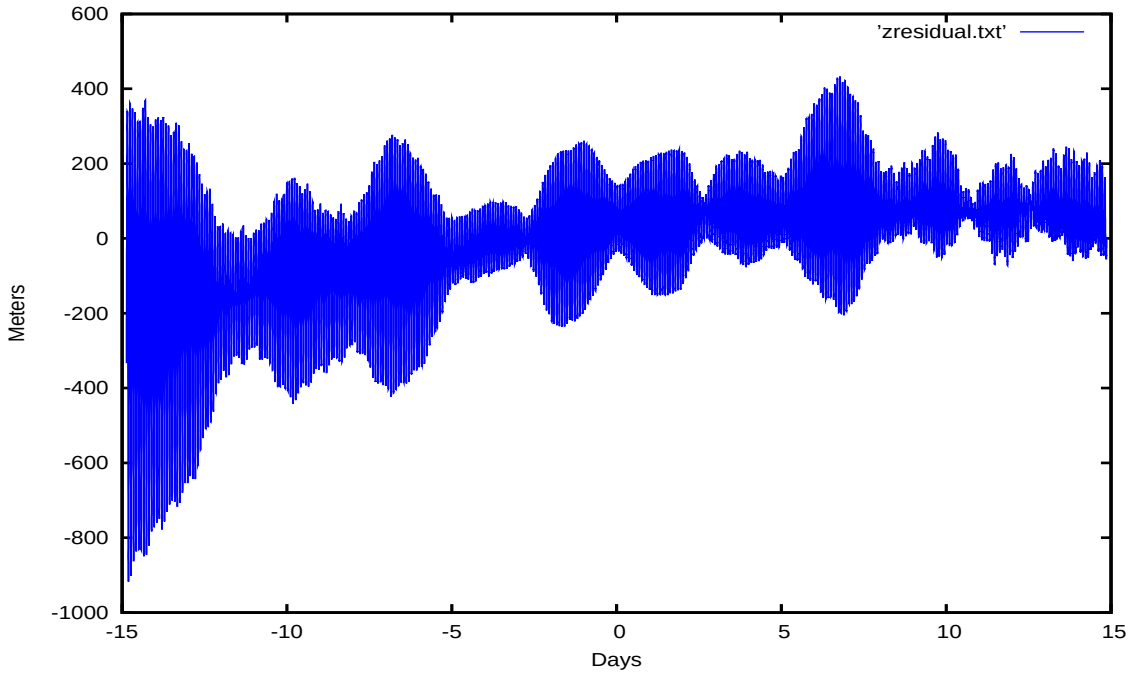

Figure C.3: The residual growth over time in the z component.

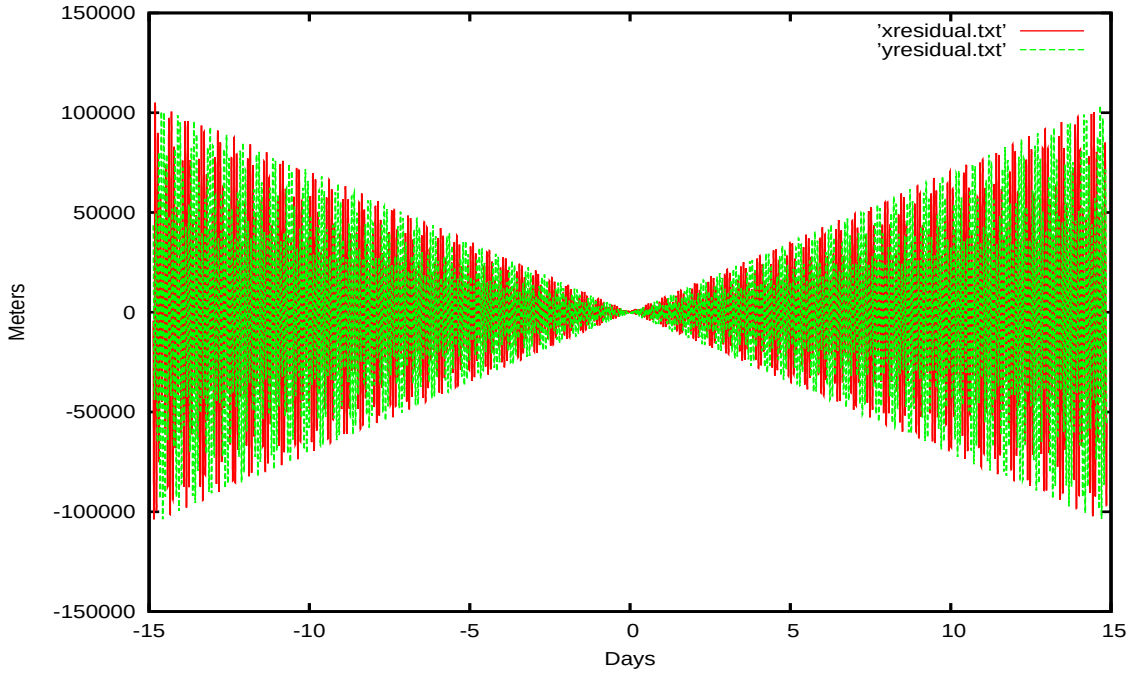

Figure C.4: The Jason-1 residuals after the frequency changes of $\delta\omega_2 = 1Eneg5\ rad/TU$.

further frequency improvements would be of lower order. The first attempt was to try $\delta\omega_2 = 2.1E-5\ rad/TU$. As seen in Figure C.6, this resulted in an increase in the residuals. This meant that the frequency adjustment was actually too high. Continuing to adjust the frequencies led to the final frequency adjustment discussed in Section 4.2.3.

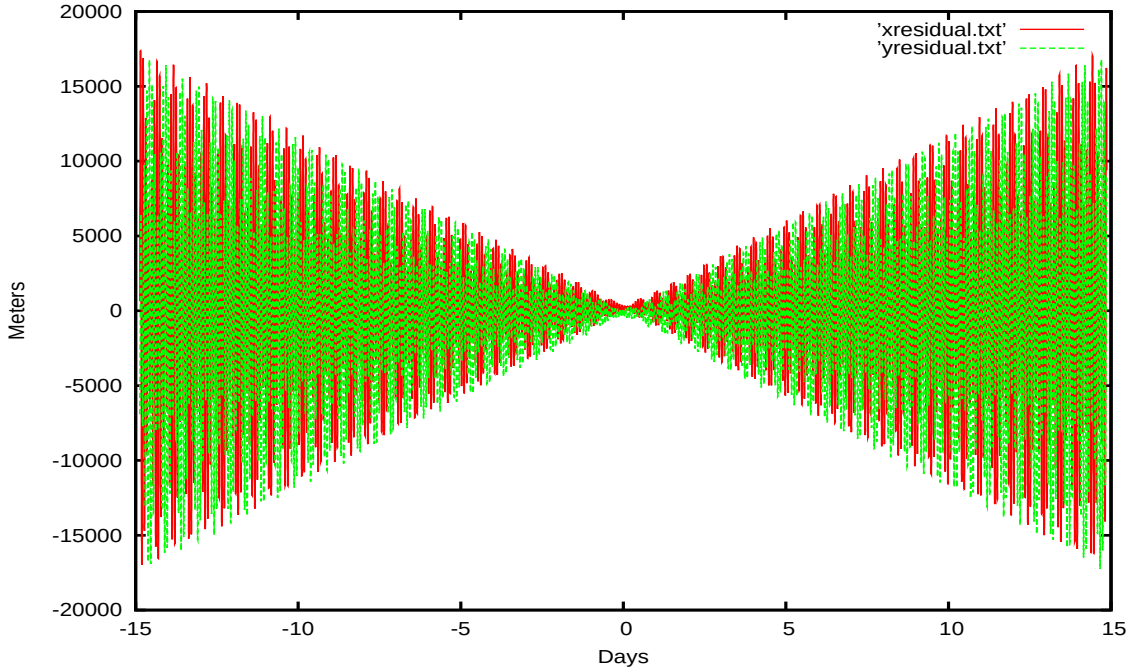

Figure C.5: The Jason-1 residuals after the frequency changes of $\delta\omega_2 = 2Eneg5\ rad/TU$.

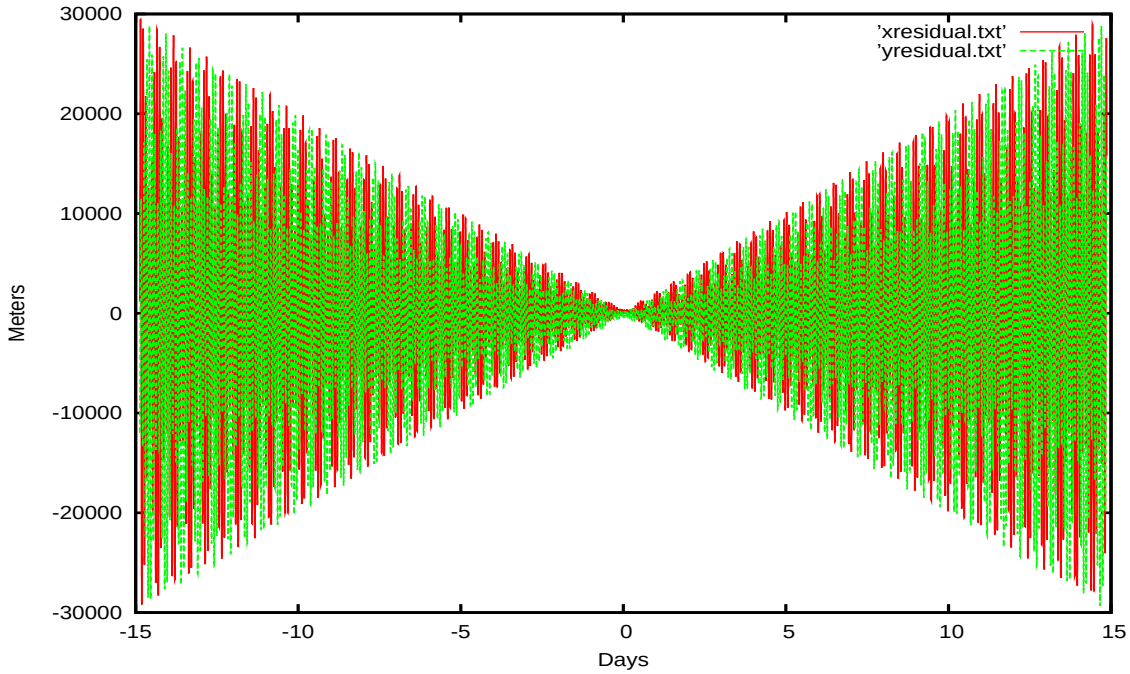

Figure C.6: The Jason-1 residuals after the frequency changes of $\delta\omega_2 = 2.1Eneg5\ rad/TU$.

Bibliography

1. "GRACE - Gravity Recovery and Climate Experiment", Aug 2007. URL `http://www.csr.utexas.edu/grace/`.

2. Arnold, V. "Proof of Kolmogorov's Theorem on the Preservation of Quasi-Periodic Motions Under Small Perturbations of the Hamiltonian". *Rus. Math. Surv.*, 18(N6):9–36, 1963.

3. Beckley, B. D., F. G. Lemoine, S. B. Luthcke, R. D. Ray, and N. P. Zelensky. "A reassessment of Global and Regional Mean Sea Level Trends from TOPEX and Jason-1 Altimetry Based on Revised Reference Frame and Orbits". *Geophysical Research Letters*, 34:L13606, 1–5, 2007.

4. Case, Kelley, Gerhard L. H. Kruizinga, and Sien-Chong Wu. "GRACE Level 1B Data Product User Handbook", Jan 2004. DRAFT.

5. Celletti, Alessandra and Luigi Chierchia. "KAM stability estimates in Celestial Mechanics". *Planet. Space Sci.*, 46(11/12):1433–1440, 1998.

6. Celletti, Alessandra and Luigi Chierchia. "KAM Stability for a Three-Body Problem of the Solar System". *Z. angew. Math. Phys.*, 57:33–41, 2006.

7. Celletti, Alessandra, Claude Froschle, and Elena Lega. "Frequency Analysis of the Stability of Asteroids in the Framework of the Restricted Three-Body Problem". *Celestial Mechanics and Dynamical Astronomy*, volume 90, 245–266. Kluwer Academic Publishers, 2004.

8. Chow, A., B. G. Williams, and Nikita Zelensky. "TOPEX/Poseiden Project NASA POE Software Interface Specification", Oct 1991. NASA Jet Propulsion Laboratory.

9. Kolmogorov, A. N. "On the Conservation of Conditionally Periodic Motions Under Small Perturbations of the Hamiltonian". *Dokl. Akad. Nauk. SSR*, 98:527–530, Jan 1954.

10. Laskar, Jacques. "introduction to frequency map analysis", 1999.

11. Laskar, Jacques. "Frequency map analysis and quasiperiodic decompositions". *proceedings of Porquerolles School*, 1–31. Astronomie et Systèmes Dynamiques, Sep 2001.

12. Laskar, Jacques and D. Robin. *Application of Frequency Map Analysis to the ALS*. Technical report, Department of Energy, Jan 1996.

13. McGill, Colin and James Binney. "Torus Construction in General Gravitational Potentials". *Mon. Not. R. Astron. Soc.*, 244:643–645, Jan 1990.

14. Moser, J. K. "On Invariant Curves of Area Preserving Mappings of an Annulus". *Nachr. der Akad. Wiss. Gottingen, Math. Phys.*, Kl. II:1:20, Jan 1962.

15. Ott, Edward. *Chaos in Dynamical Systems*. Cambridge University Press, second edition, 2002.

16. Tapley, B., J. Ries, S. Bettadpur, D. Chambers, M. Cheng, F. Condi, B. Gunter, Z. Kang, P. Nagel, R. Pastor, T. Pekker, S. Poole, and F. Wang. "GGM02 An improved Earth gravity field model from GRACE". *Journal of Geodesy*, 79(8):467–478, Nov 2005.

17. Wiesel, William E. *Modern Astrodynamics*. Aphelion Press, 1 edition, 2003.

18. Wiesel, William E. *Modern Orbit Deteermination*. Aphelion Press, 1st edition, October 2003.

19. Wiesel, William E. "Earth Satellite Orbits as KAM Tori", August 2007. Presented as paper AAS 07-423 at the AAS/AIAA Astrodynamics Specialist Conference.

20. Wiesel, William E. "KAM Tori Construction Algorithms", 2008. Unpublished.

REPORT DOCUMENTATION PAGE

Form Approved
OMB No. 0704–0188

1. REPORT DATE (DD–MM–YYYY)	2. REPORT TYPE	3. DATES COVERED (*From — To*)
26-03-2009	Master's Thesis	Sep 2007 - Mar 2009

4. TITLE AND SUBTITLE	5a. CONTRACT NUMBER
Application of KAM Theorem to Earth Orbiting Satellites	5b. GRANT NUMBER
	5c. PROGRAM ELEMENT NUMBER
6. AUTHOR(S)	5d. PROJECT NUMBER
Bryan Little, Capt, USAF	5e. TASK NUMBER
	5f. WORK UNIT NUMBER
7. PERFORMING ORGANIZATION NAME(S) AND ADDRESS(ES) Air Force Institute of Technology Graduate School of Engineering and Management (AFIT/ENY) 2950 Hobson Way WPAFB OH 45433-7765	8. PERFORMING ORGANIZATION REPORT NUMBER AFIT/GA/ENY/09-M05
9. SPONSORING / MONITORING AGENCY NAME(S) AND ADDRESS(ES) Intentionally Left Blank	10. SPONSOR/MONITOR'S ACRONYM(S)
	11. SPONSOR/MONITOR'S REPORT

12. DISTRIBUTION / AVAILABILITY STATEMENT
APPROVED FOR PUBLIC RELEASE; DISTRIBUTION UNLIMITED

13. SUPPLEMENTARY NOTES
This material is declared a work of the U.S. Government and is not subject to copyright protection in the United States.

14. ABSTRACT

An orbit that lies on a Kolmogorov, Arnold, and Moser (KAM) Torus will remain on that torus until and unless it experiences a force that causes it to leave the torus. Earth satellites that are subject only to the Earth's gravity field may lie on such KAM tori. Analyzing on orbit satellite position data should allow for the identification of the fundamental frequencies needed to define the KAM tori for modeling Earth satellite orbits.

KAM Tori are created for the Gravity Recovery and Climate Experience (GRACE) and Jason-1 satellites to model their orbital motion. Precise position data for the satellites is analyzed using a modified Laskar frequency algorithm to determine the fundamental frequencies of the orbits. The fundamental frequencies along with a set of Fourier coefficients completely describe the tori. These tori are then compared to the precise orbital position data for the satellites to determine how well they model the orbits.

The KAM torus created for the Jason-1 satellite is able to represent the position of the satellites to within 1 km. Further refinement of the torus should be possible, resulting in a more accurate model of the orbit. The GRACE torus was less successful at determining the satellite positions. Atmospheric drag cannot be ignored at the altitude where GRACE flies. It may still be possible to model GRACE with a KAM torus by applying perturbation theory to the torus; however, further research is needed to confirm this.

15. SUBJECT TERMS
Orbital Mechanics, Space Surveillance, Satellite Positioning

16. SECURITY CLASSIFICATION OF:			17. LIMITATION OF ABSTRACT	18. NUMBER OF PAGES	19a. NAME OF RESPONSIBLE PERSON
a. REPORT	b. ABSTRACT	c. THIS PAGE	UU	61	Dr. William E. Wiesel
U	U	U			19b. TELEPHONE NUMBER (Include Area Code) 937-255-6565 x4312 William.Wiesel@afit.edu

Standard Form 298 (Rev. 8–98)
Prescribed by ANSI Std. Z39.18